


Cite this: *RSC Adv.*, 2019, 9, 40588

Photoresponsive behavior of hydrophilic/hydrophobic-based novel azobenzene mesogens: synthesis, characterization and their application in optical storage devices†

Sunil B. N.,^{ab} Wan Sinn Yam^{*c} and Gurumurthy Hegde ^{*a}

Three series of alkoxy chain-bearing azobenzene-derived quaternary ammonium iodides with an alkoxy chain at one end, namely *N,N*-diethanol-6-(4-((4'-alkoxyphenyl)diazenyl)phenoxy)hexan-1-ammonium iodides, *N*-ethyl-*N*-ethanol-6-(4-((4'-alkoxyphenyl)diazenyl)phenoxy)hexan-1-ammonium iodides and *N,N*-diethyl-6-(4-((4'-alkoxyphenyl)diazenyl)phenoxy)hexan-1-ammonium iodides were synthesized and characterized. Their mesomorphic and photoswitching properties were examined *via* polarising optical microscopy (POM), differential scanning calorimetry (DSC) and UV-vis spectrophotometry. The liquid crystalline tilted schlieren texture of smectic C, non-tilted natural focal conic texture of smectic A and smectic B phases were observed in the *N,N*-diethanol- and *N*-ethyl-*N*-ethanol-bearing ammonium group substituted at the terminal *via* the alkoxy chain of the azo moiety. In these azo moieties, the equilibrium time for *trans*–*cis* isomerization was about 1 min and *cis*–*trans* isomerization occurred at around 590 min, which had the highest alkoxy chain and no hydroxyl group on their head group. The absence of a hydroxyl group on the terminal head group resulted in slow thermal back relaxation, whereas the hydroxyl group-bearing head group showed fast thermal back relaxation. These results suggest that the influence of the substituent on the cationic ammonium head group and alkoxy chain length on the photoisomerization of the azo compounds is vital for optical storage devices. Furthermore, the device fabricated using these materials demonstrated that they are excellent candidates for optical image storage applications.

Received 9th October 2019
Accepted 10th November 2019

DOI: 10.1039/c9ra08211e

rsc.li/rsc-advances

1 Introduction

Optical storage devices have attracted increasing attention in the field of information technology over the last few years.^{1–5} Organic photochromic compounds are used to evaluate the photoinduced behaviour of optical storage devices.^{6,7} This process arises from the reversible photoinduced isomerization of a photochromic group such as azobenzene. The azobenzene chromophore is a good candidate for storing data optically due to its photosensitivity and good photoisomerization properties.^{8–11} Upon UV illumination (~365 nm related to the π – π^* transition), its thermodynamically more stable rod-like molecular form of *E* or *trans* isomer is converted into the bent *Z* or *cis* isomer. Reverse *cis*–*trans* isomerization can be achieved *via* illumination under visible light (~400–500 nm, related to the n –

π^* transition). This reverse transformation can also occur in the “dark” *via* a process known as thermal back relaxation.^{12,13} The decoration of different functional groups on the azobenzene chromophore has been studied to enhance its optical storage properties.^{14–21}

Ionic liquids have been developed in the past two decades because of their unique physicochemical properties and highly tunable features with chemical modification.^{22–25} Thus, it is possible to design functionalized azobenzene-based ionic liquids by introducing quaternary ammonium salts into the photoresponsive unit of azobenzene.^{26,27} In this context, some azobenzene-based ionic liquids have been designed and used in many applications such as catalysis,²⁸ sensors,²⁹ drug delivery³⁰ and coatings.³¹ Based on a recent literature survey,^{32–34} azobenzene-based ionic liquids are rarely used in the field of optical storage devices. In recent years,^{35–37} some photo-responsive ionic liquids have been reported. The azobenzene-based ionic liquid 4-butylazobenzene-40-hexyloxytrimethylammonium trifluoroacetate ([C₄AzoC₆TMA] [TfO]) with an azobenzene unit bridged between the alkyl chain has been synthesized and its reversible micelle-vesicle transformation under UV-vis illumination studied.³⁸ Similarly, the synthesis

^aCentre for Nano-materials and Displays, B.M.S. College of Engineering, Bull Temple Road, Bengaluru 560019, India. E-mail: murthyhegde@gmail.com

^bDepartment of Chemistry, B.M.S. College of Engineering, Bangalore, India 560019

^cSchool of Chemical Sciences, Universiti Sains Malaysia, 11800 USM Penang, Malaysia. E-mail: wansinn@usm.my

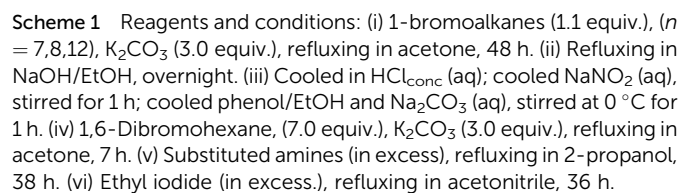
† Electronic supplementary information (ESI) available. See DOI: 10.1039/c9ra08211e



This study provides useful information for creating optical storage devices by understanding the structure–property relationship of azobenzene-based ionic liquids. The photoisomerization and liquid crystalline properties of the intermediates were also studied for a better understanding between them.

2.1 Synthesis

4-Acetamidophenol was *O*-alkylated using 1-bromoalkanes to produce 4-acetamidophenoxyalkanes (**1–3**) and further refluxed with alcoholic sodium hydroxide to give 4-alkyloxylanilines (**4–6**). The 4-alkyloxylanilines were diazotized with sodium nitrite and conc. HCl at 0 °C and the diazonium solution was treated with phenol in the presence of sodium carbonate to obtain the coupled products **7–9**. Compounds **7–9**

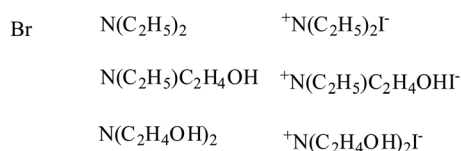


were treated with 1,6-dibromohexane, and refluxed overnight under a nitrogen atmosphere to obtain compounds **10–12**, and then reacted with substituted amines to produce **13–21**. Compounds **22–30** were obtained upon treatment with ethyl iodide. The crude product was recrystallized from a mixture of ethanol/*n*-hexane and characterized using ¹H-NMR, ¹³C-NMR, HRMS and elemental analyses.

The bromo group was substituted at the terminal end (*via* the alkoxy chain) of azobenzene derivatives **7–8** bearing different alkoxy chain lengths on the other end of the phenyl ring. The bromo group was fixed at one end and the alkoxy chain varied at the other end of compounds **10–12**. The push–pull type effect

where, $n = 7, 8, 12$

R= Bromo, tertiary amine, quaternary ammonium salt



RSC Adv., 2019, 9, 40588–40606 | 40589

was observed in these types of molecules due to the presence of the bromo group, which acts as an electron withdrawing group, whereas, the alkoxy chain acts as an electron donating group. The influence of the alkoxy chain and bromo group on the mesomorphic and photoswitching properties of the azobenzene chromophore were studied in detail.

2.2.1 Mesomorphic studies. Mesomorphic studies on **10–12** were performed using polarizing optical microscopy (POM) in the crystalline phase upon heating at the rate of 2 °C per min. The azobenzene-based mesogen formed different types of enantiotropic mesophases with phase sequences depending on the alkoxy chain length (see Table 1). Compounds **10** and **12** exhibited a non-tilted smectic (SmA) phase, while compound **11** formed tilted an SmC phase along with an SmA phase.

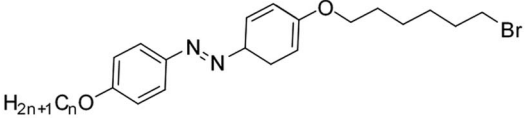
Fig. 2 shows the natural focal conic texture, which is typical of the SmA phase, exhibited by compounds **10–12** at the respective temperatures. The phase transition temperature and enthalpy changes were determined *via* differential scanning calorimetry (DSC) upon heating at 5 °C min^{−1}. A summary of the phase transition temperatures, mesophase types and transition enthalpies is given in Table 1. The DSC thermograms are presented in the ESI.†

2.2.2 Photoswitching properties. The photoswitching studies on intermediates **10–12** were performed using a UV-vis spectrophotometer with a quartz cuvette and chloroform as the solvent. Before UV illumination, compounds **10–12** showed

a strong absorption peak at the wavelength of 359–360 nm and weak band at ~450 nm, which correspond to the symmetry allowed $\pi-\pi^*$ transition and symmetry forbidden $n-\pi^*$ transition, respectively. There was no notable difference among the absorption spectra of compounds **10–12** due to their similar chemical architecture. Therefore, an increase in the length of the alkoxy chain does not affect the wavelength of the absorption spectrum.

During UV illumination, the typical maximum absorption wavelength at 359 nm disappeared, while a peak appeared at ~450 nm due to an increase in the content of *cis* isomer. The isomerisation process of **10** was recorded as a function of UV irradiation time. Compounds **10–12** took around 44 s to reach the photoequilibrium state and upon further continuous irradiation of UV light up to 60 s, there were no changes in their absorption spectra. This suggests the *trans* isomer reached its equilibrium state of isomerization reaction. After reaching the photostationary state, the thermal back relaxation of the *cis-trans* isomerization was examined by keeping the samples in the dark. Among them, compound **11** showed a good thermal back relaxation time of about 590 min, whereas, **10** showed a fast back relaxation time of ~100 min. The normalized absorption spectra upon UV illumination and thermal back relaxation of **10–12** are shown in Fig. 3 and 4, respectively. The peak absorbance graph was plotted as a function of time by extracting data from the absorption spectra of compounds **10–12**. Graphs (a and b) (in

Table 1 Phase transition temperatures, mesophase types, and transition enthalpies [$\Delta H/\text{kJ mol}^{-1}$] of compounds **10–12** upon heating^a

		
Compound code	<i>n</i>	Phase transitions <i>T</i> /°C [$\Delta H/\text{kJ mol}^{-1}$]
10	7	H: Cr 103.80 [54.46] SmA 111.77 [0.92] Iso
11	7	H: Cr 95.69 [50.96] SmC 109.67 (1.90) SmA 113.54 [1.14] Iso
12	12	H: Cr 100.03 [77.0] SmA 112.29 (9.73) Iso

^a Transition temperatures and enthalpy values were taken from the DSC heating (H) scans at 5 °C min^{−1}; abbreviations: Cr = crystalline solid; SmA = smectic phase A phase; SmB = smectic B phase; SmC = smectic C phase; and Iso = isotropic liquid.

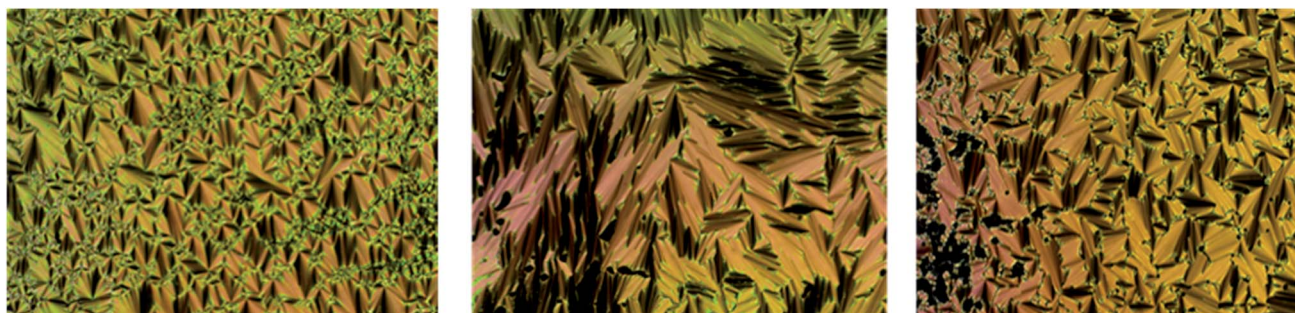


Fig. 2 The SmA phase exhibiting the natural focal conic texture as seen in compound **10**, **11** and **12** at respective temperatures. Magnification used is 10×.



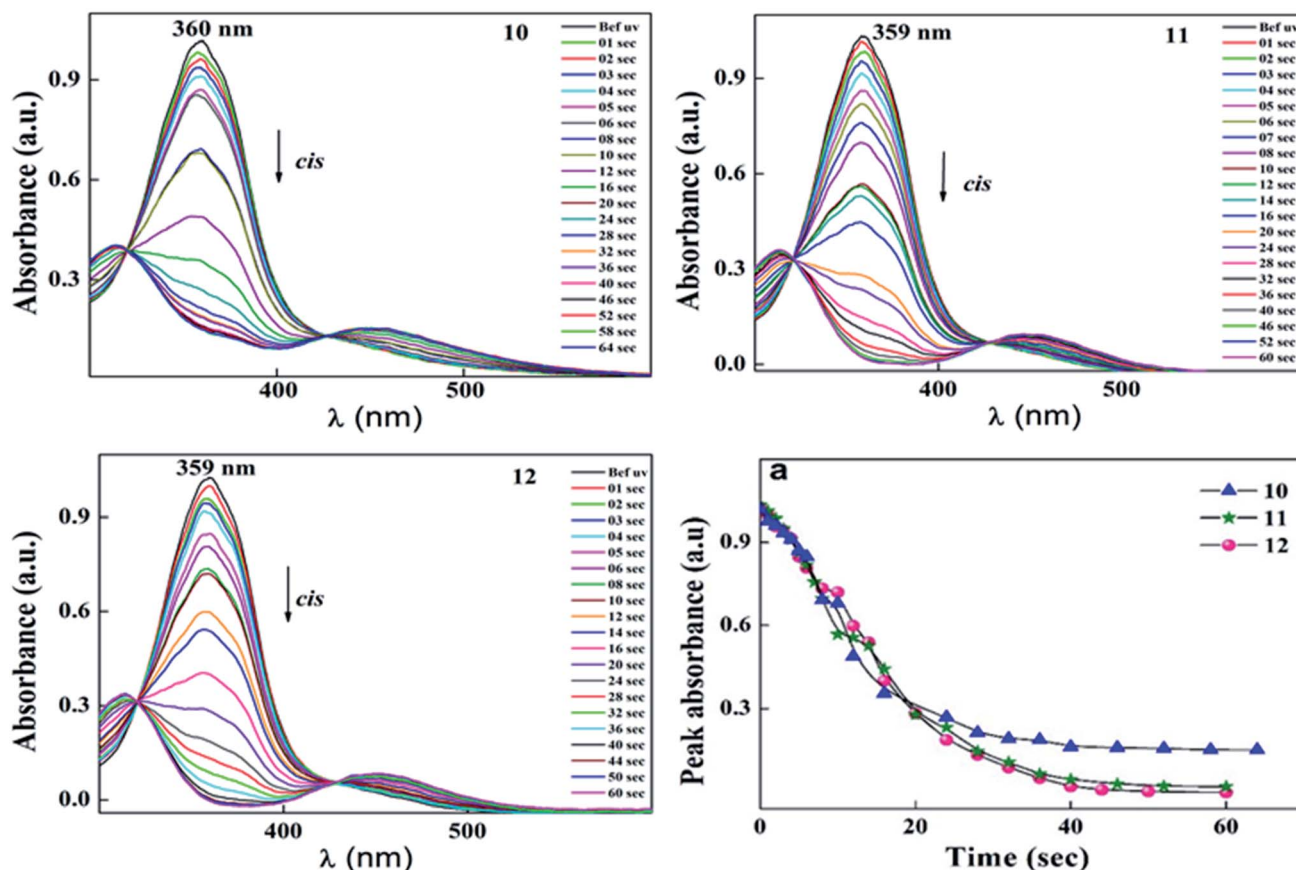


Fig. 3 Normalized absorption spectra of compounds 10–12 as a function of UV irradiation time and graph (a) represents a peak absorbance plot for *trans*–*cis* isomerization, extracted from the absorption spectra (in this figure) of 10–12. Intensity of the UV illumination was 1 mW cm^{-2} .

Fig. 3 and 4, respectively) show the peak absorbance graph of UV illumination and thermal back relaxation of compounds 10–12 with respect to irradiation time and recovery time, respectively.

For *trans*–*cis* isomerization of 10–12, the equilibrium state of the *E/Z* isomer ratio was dependent on the wavelength. After exposure to a wavelength of 365 nm, conversion efficiency of the *trans* isomer was around 90%. Considering the case of sample 12, the conversion efficiency of *trans*–*cis* isomerization was 99%, whereas, 10 showed 85%. After 40 s UV irradiation, the conversion efficiency of these compounds remained the same. The photoconversion efficiency of the *trans*–*cis* isomerisation was determined using eqn (1).⁴⁰

$$\text{CE} = \frac{A_{(t_0)} - A_{(t_\infty)}}{A_{(t_0)}} \quad (1)$$

where CE is the conversion efficiency, and $A_{(t_0)}$ and $A_{(t_\infty)}$ are absorbance before and after UV illumination, respectively. A summary of the *trans*–*cis* isomerization time, thermal back relaxation of *cis*–*trans* isomerization and photoconversion efficiency data is shown in Table 2.

2.3 Azobenzene-mesogen bearing a terminal tertiary amine group

The bromo group was replaced by *N,N*-diethanol, *N*-ethyl-*N*-ethanol, and *N,N*-diethyl containing an amine group at the

terminal with the same alkoxy chain length of intermediates 10–12 at one end, and the other end of the azo ring bearing different alkoxy chain lengths. The mesomorphic and photo-switching properties of intermediates 13–21 were investigated here. These types of compounds exhibited a push–push type effect due to the electron donating nature of both groups present in the side chain. The influence of the hydrophobic and hydrophilic nature of the substituted tertiary amine on the mesomorphism and photoisomerization properties were extensively studied.

2.3.1 Mesomorphic studies. The liquid crystalline properties of intermediates 13–21 were examined similarly to 10–12 using POM and DSC. Three types of enantiotropic phases were observed in the *N,N*-diethanol, *N*-ethyl-*N*-ethanol, and *N,N*-diethyl substituted amine compounds. The *N,N*-diethanol substituted amine 15 exhibited schlieren texture of smectic C and smectic B phases, whereas, in the case of the *N*-ethyl-*N*-ethanol amine-bearing compound 18, it showed smectic C and smectic A phases upon heating. The polarizing optical images are shown in Fig. 5 together with the representative mesophase of SmC and SmB for compounds 18 and 15 at the respective temperature. However, the compounds possessing the highest alkoxy chain ($n = 12$) showed mesophases, whereas, the other two lower alkoxy homologues ($n = 7$ and 8) were non-mesogenic in nature. The *N,N*-diethyl amine group-containing compounds



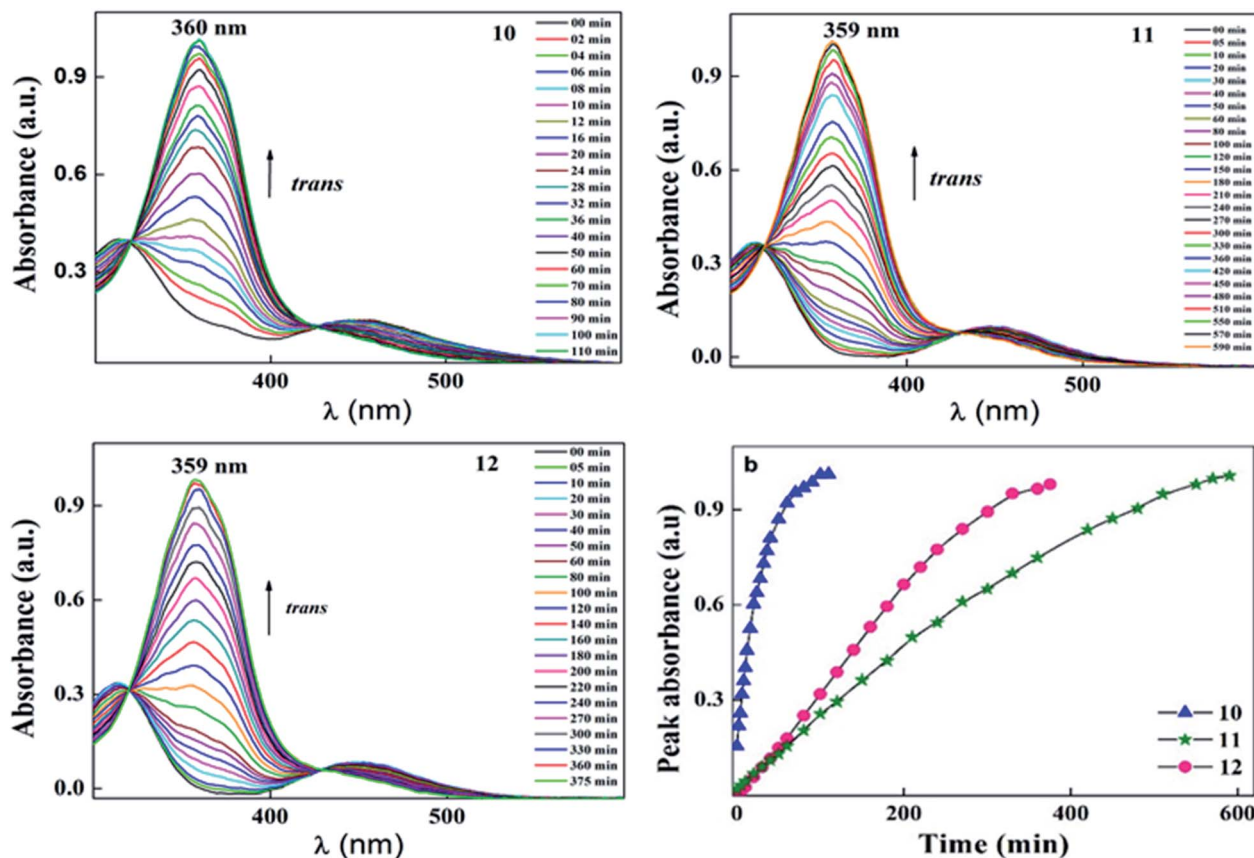


Fig. 4 Normalized absorption spectra of compounds 10–12 as a function of recovery time during thermal back relaxation and graph (b) represents the peak absorbance plot for *cis*–*trans* isomerization, which was extracted from the absorption spectra (Fig. 4) of 10–12.

Table 2 A summary of the *E/Z* isomerisation, thermal back relaxation and its photoconversion efficiency (CE %) data

Compound code	<i>trans</i> – <i>cis</i> isomerization in s	Thermal back relaxation in min	CE %
10	44	100	85.67
11	44	590	98.25
12	44	375	99.20

19, 20 and 21 also did not show liquid crystalline phases due to the hydrophobic nature of the substituted group on the tertiary amine. This information is vital to achieve mesomorphicity when tuning the alkoxy homologues.

A summary of the phase transition temperature and transition enthalpies are given in Table 3. The DSC thermograms for all the compounds are given in the ESI.†

2.3.2 Photoswitching properties. The UV-vis investigation showed the influence of *N,N*-diethanol, *N*-ethyl-*N*-ethanol, *N,N*-diethyl containing an amine group on the isomerisation of intermediates 13–21. The photoisomerization of 13–21 was examined similarly to 10–12. The normalized absorption spectra upon UV illumination and thermal back relaxation of intermediates 13–21 are shown in Fig. 6 and Fig. 7, respectively. The peak absorbance graph was plotted similarly to 10–12, and

Fig. 8 shows the peak absorbance plots upon UV illumination (graph (c)) and thermal back relaxation (graph (d)) with respect to time. As Fig. 8 suggests, reversible isomerization depends on the alkoxy chain and substituted groups on the nitrogen atom of the amine group. The thermal back relaxation time increased as the length of the alkoxy chain increased. The presence of a hydroxyl group on amine resulted in fast-thermal back relaxation, whereas, it was slow in the case of the alkyl chain substituted amine. For example, the *N,N*-diethanol amine-based azobenzene with a terminal alkoxy chain length of $n = 8$ reached photosaturation at a time of ~ 80 s, whereas, its thermal back relaxation was about 240 min. A summary of the *E/Z* isomerisation, thermal back relaxation time and its photoconversion efficiency of intermediates 13–21 are given in Table 4.

The photoconversion efficiency of *E/Z* isomerisation was determined using eqn (1). The photoconversion efficiency of intermediates 13–21 was more than 90%, indicating that the thermally stable *trans* isomer was converted to the unstable *cis* isomer to a great extent. In the case of compounds 13–18, conversion of the *trans* isomer to the *cis* isomer took more time compared to that for 19–21 due to the presence of a hydroxyl group on the amine group. The intermolecular hydrogen bonding effect of the hydroxyl group increased the equilibrium time for the isomerization reaction.



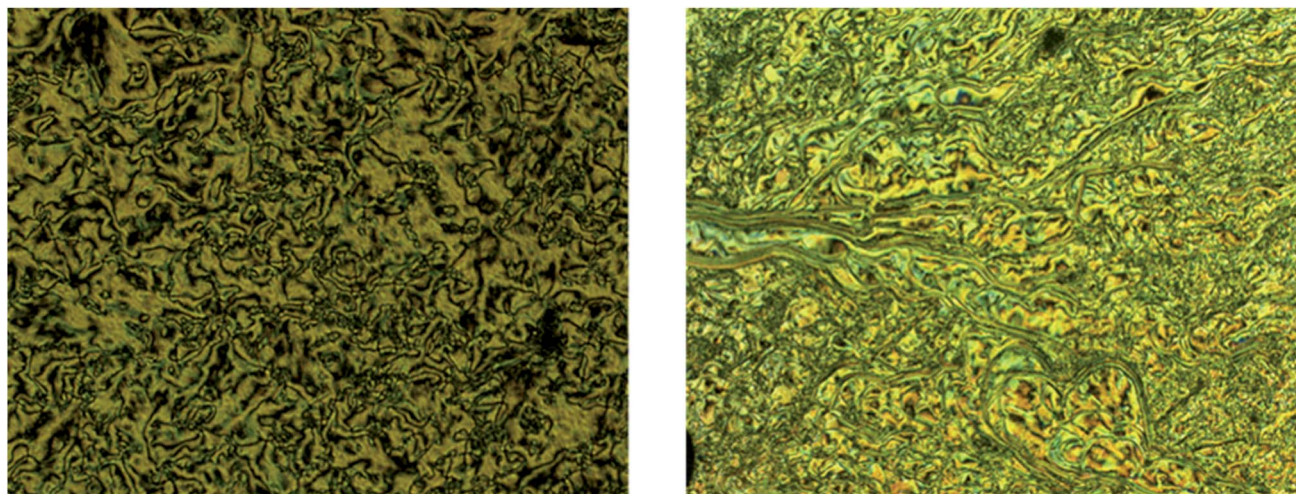


Fig. 5 Schlieren texture of SmC phase observed in compound **18** (left) and SmB phase for compound **15** (right) magnification 10 \times .

2.4 Azobenzene mesogen bearing a terminal quaternary ammonium group

Azobenzene is the most efficient and extensively studied chromophore, where azobenzene derivatives with the *trans* isomer are thermodynamically more stable than that with the *cis* isomer. In this section, we present the mesomorphic and photoswitching properties of the quaternary ammonium salt bearing alkoxy azobenzene. Generally quaternary ammonium salts are called cationic surfactants, which are prepared by adding an ethyl group to the nitrogen atom of a tertiary amine. Similarly, the quaternary ammonium group-based azobenzene derivatives were prepared by adding an ethyl group to the terminal tertiary amine of intermediates **13**–**21**. The mesomorphic properties and photo-induced isomerization of the azobenzene-based mesogen-bearing cationic surfactants (**22**–**30**) were examined in detail.

2.4.1 Mesomorphic studies. The liquid crystalline properties of compounds **22**–**30** were examined similarly to the intermediates. Enantiotropic and monotropic phases were observed in the *N,N*-diethanol and *N*-ethyl-*N*-ethanol quaternary ammonium salts bearing alkoxy azobenzene. The *N,N*-diethanol quaternary ammonium salt exhibited enantiotropic phases such as smectic C and smectic B phases upon heating. In the case of the *N*-ethyl-*N*-ethanol quaternary ammonium salt **24**, it exhibited monotropic phases (schlieren texture of SmC phase) as shown in Fig. 9a.

The natural focal conic texture exhibiting the SmA phase of compound **26** and the SmC phase of compound **27** are shown in Fig. 9b and c, respectively. The *N,N*-diethyl quaternary ammonium salt-based azobenzenes are non-liquid crystalline in nature due to the absence of a hydroxyl group on their head group. Hence, the mesophases changes in their properties may

Table 3 Phase transition temperatures, mesophase types, and transition enthalpies [$\Delta H/\text{kJ mol}^{-1}$] of compounds **13**–**21** upon heating^a

Compound code	<i>n</i>	R'	R''	Phase transitions <i>T</i> /°C [$\Delta H/\text{kJ mol}^{-1}$]
13	7	–OH	–OH	H: Cr 106.37 [24.18] Iso
14	8	–OH	–OH	H: Cr 107.31 [27.29] Iso
15	12	–OH	–OH	H: Cr 82.92 [21.49] SmC 99.26 [13.82] SmB 115.08 [13.04] Iso
16	7	–OH	–H	H: Cr 73.28 [18.76] Iso
17	8	–OH	–H	H: Cr 74.51 [19.97] Iso
18	12	–OH	–H	H: Cr 87.79 [37.55] SmC 104.46 [4.81] SmA 115.52 [2.72] Iso
19	7	–H	–H	H: Cr 81.72 [16.15] Iso
20	8	–H	–H	H: Cr 79.55 [13.91] Iso
21	12	–H	–H	H: Cr 79.76 [44.32] Iso

^a Abbreviations see Table 1.



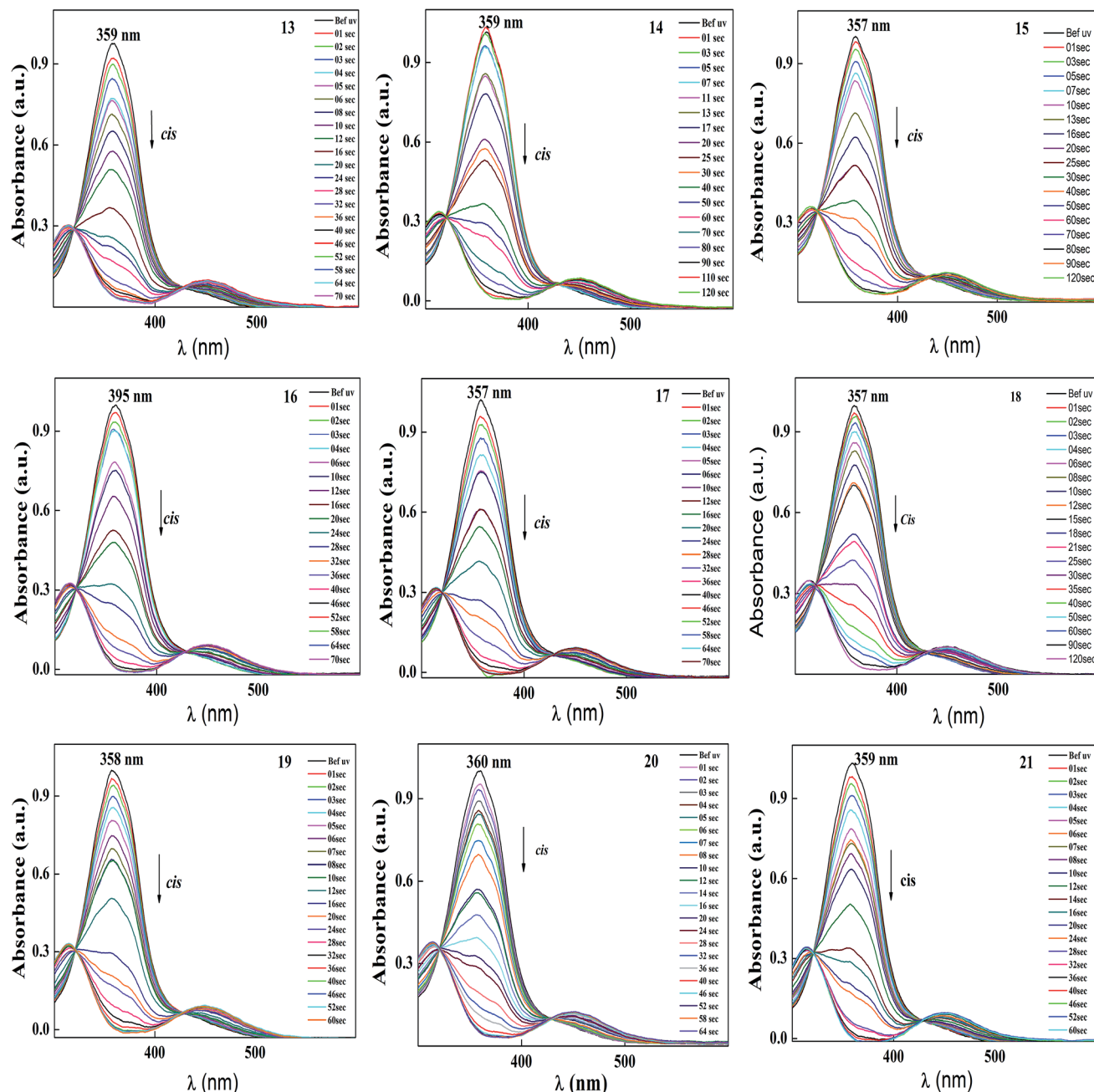


Fig. 6 Normalized absorption spectra of compound 13–21 as a function of UV irradiation time. Intensity of the UV illumination is 1 mW cm^{-2} .

be due to the polar group present in the quaternary ammonium salt. The phase transition temperature and transition enthalpies were determined *via* DSC and the summarized data given in Table 5.

To better understand the mesophases, the proposed model, as shown in Fig. 10 shows the formation of non-tilted smectic A and tilted smectic C phases. The smectic A mesophase was observed in all the compounds bearing a hydroxyl group on their terminal head group. The influence of the terminal alkoxy chain ($n > 10$) length on the formation of ionic liquid crystals with the smectic C phase was previously reported.⁴¹ According to the zigzag model by Wulf,⁴² the appearance of the smectic C

phase occurs by increasing the length of the terminal chain. For compounds 24 and 27, which have the highest chain length at the terminal end ($n = 12$), evidence was observed for the formation of the smectic C phase and also similar results were observed in the case of compounds 15 and 18. In the case of the substituent $X = \text{H}$ on the head group, no liquid crystalline properties were observed because the hydroxyl group plays a major role in the mesomorphism.

2.4.2 Photoswitching properties. The photoswitching studies of the azobenzene-mesogen-bearing ionic liquids were investigated similarly to the intermediates. Before and after UV illumination, the absorption spectra of 22–30 were recorded by



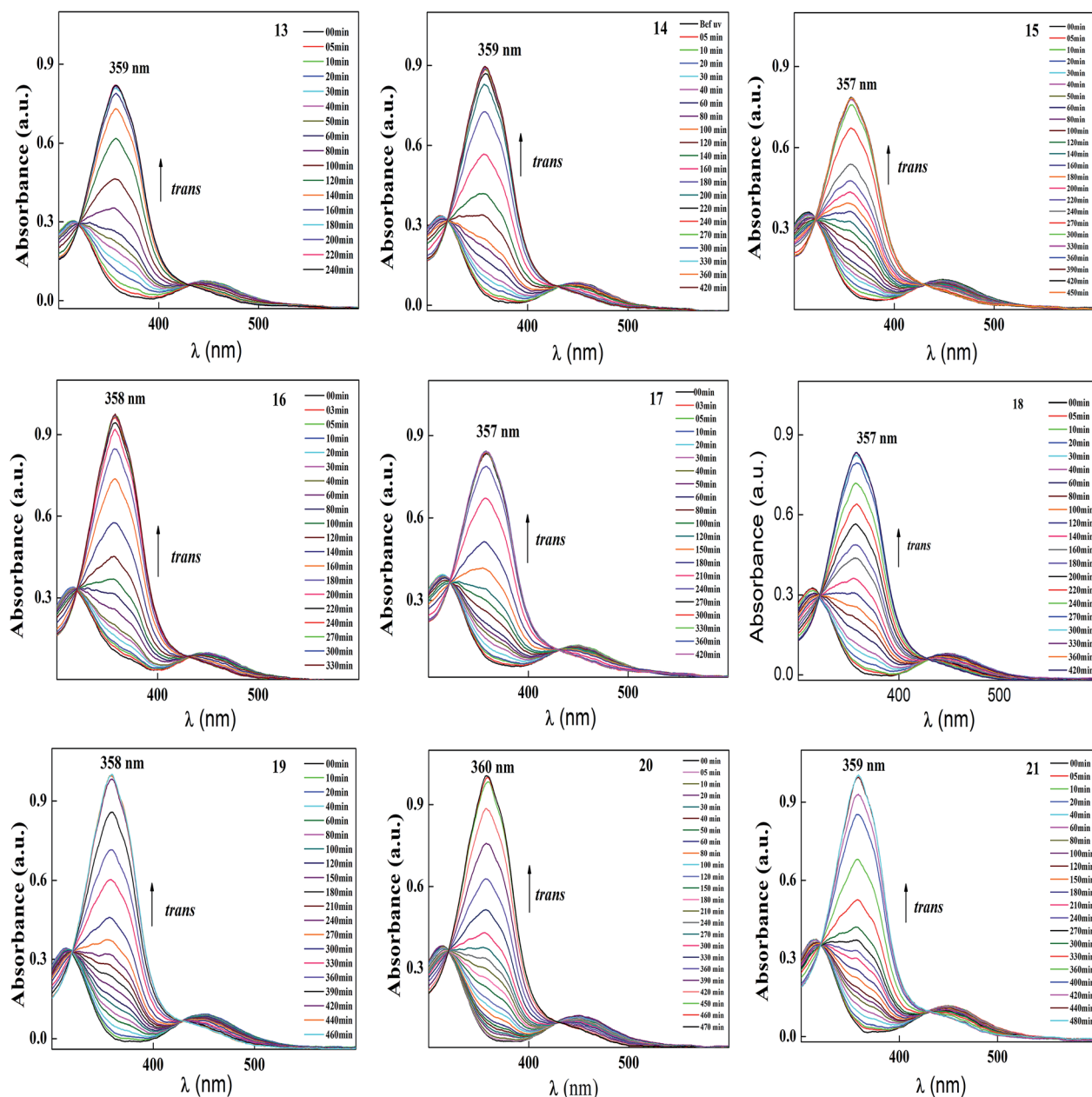


Fig. 7 Normalized absorption spectra of compounds 13–21 as a function of recovery time during thermal back relaxation.

UV-vis spectroscopy. There were no notable changes in the peak wavelength, and the characteristic peak absorption wavelength at 356–359 nm originated from the π - π^* transition of the *trans* isomer. After UV irradiation, the absorption peak at 356 nm gradually decreased due to the transformation of the *cis* isomer for compound 22. After 25 s of irradiation, the *trans* isomer reached the photo equilibrium state in the isomerization reaction.

After reaching the photosaturation state, the reverse transformation of the *cis* isomer occurred in the dark and the thermal back relaxation was recorded with respect to the recovery time of the *trans* isomer. Similar results were also observed to that of the other compounds, and the normalized

absorption spectra of compounds 22–30 are given in Fig. 11. The peak absorbance *versus* time was plotted by extracting data from the absorption spectra of compounds 22–30 upon UV illumination as shown in graph (e) (see Fig. 11). The photo-conversion efficiency for *trans*-*cis* isomerization of the azobenzene-based ionic liquids was determined using eqn (1). All the compounds showed good conversion efficiency, suggesting the ionic liquids exhibit quick photoresponsive behaviour in solution. In the case of compound 30, the conversion efficiency was about 94%, whereas, compound 27 showed 66%. The presence of a hydroxyl group on the head group reduced the *cis* isomer ratio in the photoequilibrium state during photo-isomerization. Therefore, the presence of a hydroxyl group and



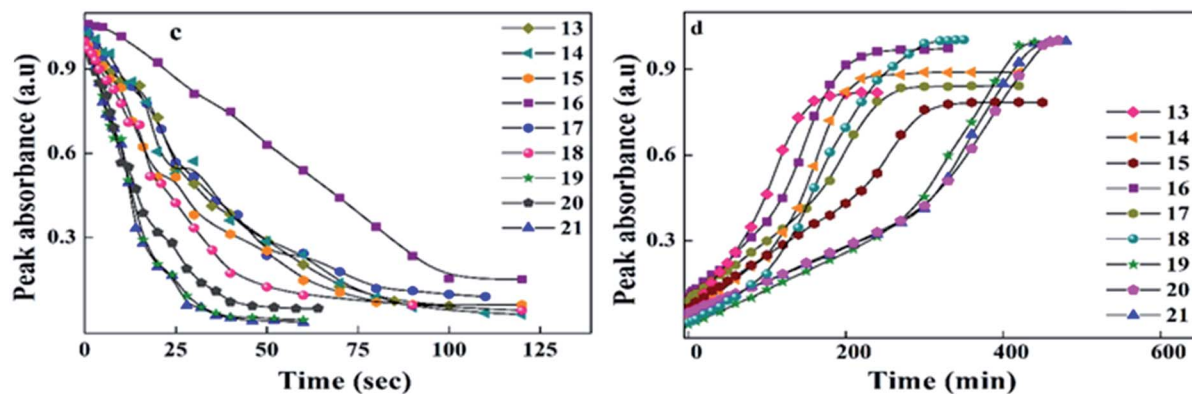


Fig. 8 Peak absorbance with respect to time graph (c) peak absorbance plot for *trans*–*cis* isomerization, with the data extracted from the absorption spectra (Fig. 6) of 13–21 during UV illumination and graph (d) peak absorbance plot for *cis*–*trans* isomerization, with the data extracted from the absorption spectra (Fig. 7) of 13–21 during thermal back relaxation.

Table 4 The summarized data of *E/Z* isomerisation, thermal back relaxation and its photoconversion efficiency

Compound code	<i>E/Z</i> isomerization in s	Thermal back relaxation in min	CE %
13	70	180	96.00
14	80	240	96.77
15	85	330	94.47
16	90	240	99.49
17	85	270	98.92
18	56	320	94.47
19	40	440	99.82
20	46	460	95.20
21	52	440	94.96

the alkoxy chain length play a significant role in photoisomerization. A summary of the photoconversion efficiency data for the *trans*–*cis* isomerization is shown in Table 6.

Among all the compounds, **30** showed the best thermal back relaxation time of about 590 min, whereas, the *cis* isomer of compound **22** was not fully transformed into the *trans* isomer. The terminal head group of the azobenzene unit acts as an

electron withdrawing group, which can reduce the isomerization energy barrier and accelerate the isomerization of azobenzene. However, in the case of **22**, the presence of a hydroxyl group reduced the electron withdrawing character of the head group. As a result, the *cis* isomer was not fully converted into its original state and also could be phase involved during thermal back relaxation due to the molecules being arranged in an ordered layer structure (smectic phase). Furthermore, the normalized absorption spectra for the thermal back relaxation of the azobenzene-based ionic liquids were investigated in detail (Fig. 12). According to Fig. 12, after the photoequilibrium state, the *cis* isomer of **22**–**27** did not fully transform back to its original state due to the formation of intermolecular hydrogen bonding in the hydroxyl group present on its head group.

A schematic diagram of the light-induced photoisomerization of the azo compounds is shown in Fig. 13. The polar substituent ($X = OH$) on the head group of the azo compounds of the *cis* isomer could not achieve its original state due to the layered arrangement of molecules (smectic A phase) restricting the free rotation of the molecule during thermal back relaxation. In the case of **29** and **30**, they possess random arrangements due to the absence of a hydroxyl group on their head group and they exhibited long thermal back relaxation.

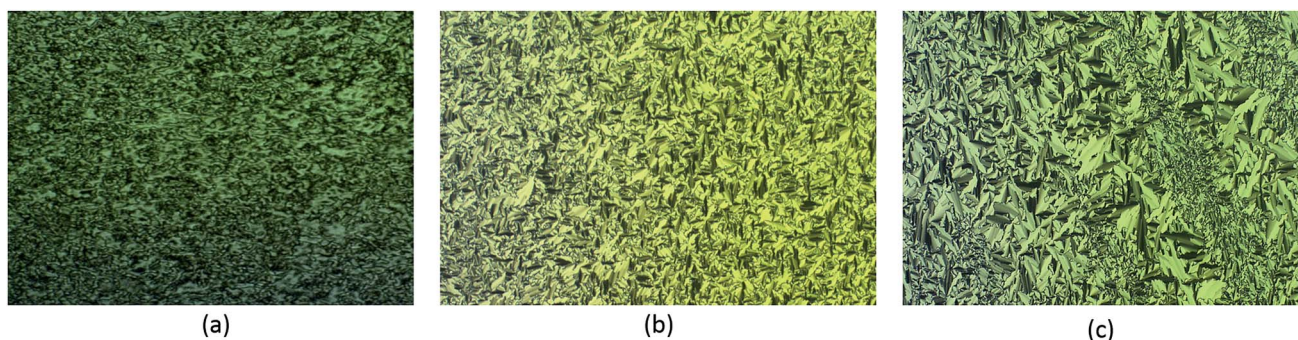
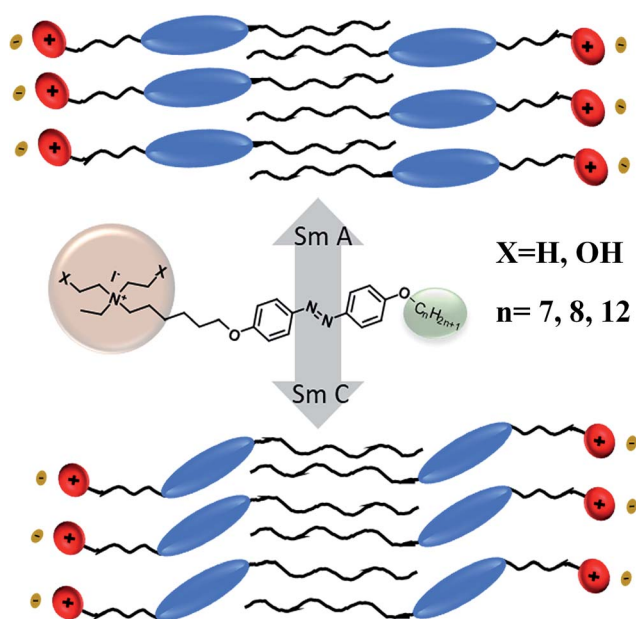


Fig. 9 Polarized optical images. (a) Schlieren texture of SmC phase observed in compound **24**, (b) natural focal conic texture typical of SmA for compound **26** and (c) SmC phase as seen in compound **27**. Magnification used is 10 \times .



Table 5 Phase transition temperatures, mesophase types, and transition enthalpies [$\Delta H/\text{kJ mol}^{-1}$] of compounds **22–30** upon heating^a

Compound code	<i>n</i>	R'	R''	Phase transitions <i>T</i> /°C [$\Delta H/\text{kJ mol}^{-1}$]
22	7	–OH	–OH	H: Cr 143.04 [38.48] SmA 222.92 [3.57] Iso
23	8	–OH	–OH	H: Cr 141.0 [13.80] SmA 220.92 [2.22] Iso
24	12	–OH	–OH	H: Cr 135.98 [45.11] SmC 132.15 [1.66] SmA 194.17 [3.32] Iso
25	7	–OH	–H	H: Cr 158.09 [42.26] SmA 185.98 [0.91] Iso
26	8	–OH	–H	H: Cr 148.91 [32.42] SmA 199.56 [0.89] Iso
27	12	–OH	–H	H: Cr 52.81 [11.23] SmC 111.71 [6.64] Iso
28	7	–H	–H	H: Cr 81.72 [21.53] Iso
29	8	–H	–H	H: Cr 142.92 [11.98] Iso
30	12	–H	–H	H: Cr 174.19 [29.18] Iso

^a Abbreviations: see Table 1.**Fig. 10** Proposed model showing the appearance of liquid crystalline phases (SmA and SmC phases).

2.5 Kinetic studies

For azo compounds **10–30**, it is necessary to study the kinetics of their *cis–trans* isomerisation, which was carried out thermally using UV-vis spectroscopy.⁴³ The experiment was carried out in the dark at room temperature of 27 °C and chloroform was used as the solvent. The unimolecular thermal *cis–trans* isomerisation in the dark obeys eqn (2).

$$-K_{c \rightarrow t}t = \ln \frac{A_{(\infty)} - A_{(t)}}{A_{(\infty)} - A_{(0)}} \quad (2)$$

where A_t , A_0 and A_∞ are the change in absorbance at time t , time zero and infinite time, respectively. t is the relaxation time of the

respective *cis* isomer. The time region in Fig. 14 shows that the reaction is first order in the case of **10**, whereas in the case of **11** and **12**, the reactions are first order at a certain time and thereafter, due to the long thermal back relaxation it is deviated from first order to second order kinetics. During thermal back relaxation, temperature may play a significant role in deviating from first order.⁴⁰ As shown in Fig. 14, the reaction is first order at a certain time and deviates to second order due to the *cis* isomer being thermally stable for some time due to the push–pull-type of effect arising in compounds **13–21**.

In the case of compounds **22–30**, most of the reaction is first order except for compound **30**, which exhibited a push–pull-type effect due to the head group of the ionic liquid acting as an electron withdrawing group. In the case of **22–27**, the reaction was first order due to the presence of a hydroxyl group exhibiting the pull–pull-type effect, which could not reduce the isomerization energy barrier and the acceleration of the isomerization of azobenzene was negligible.

2.6 Optical storage device

Spectral investigation on a real device was also conducted to determine the potential of the materials. Fabrication of the cell involved ITO coated, polyimide rubbed sandwiched glass plates with the desired thickness of around $\sim 5 \mu\text{m}$. The guest–host mixture was prepared, where azobenzene molecules acted as the guest and the room temperature liquid crystal acted as the host material.

As a representative compound, we took compound **30** as our guest light sensitive molecules since it showed the best properties during the photoisomerization studies. The mixture consisted of 5% of compound **30** (which is a light-sensitive molecule but non-liquid crystalline in nature) mixed with 95% MLC-6873-100 (room temperature commercial liquid crystal). This mixture exhibited a room temperature nematic mesophase. The prepared mixture was capillary filled in a cell, which was previously fabricated.



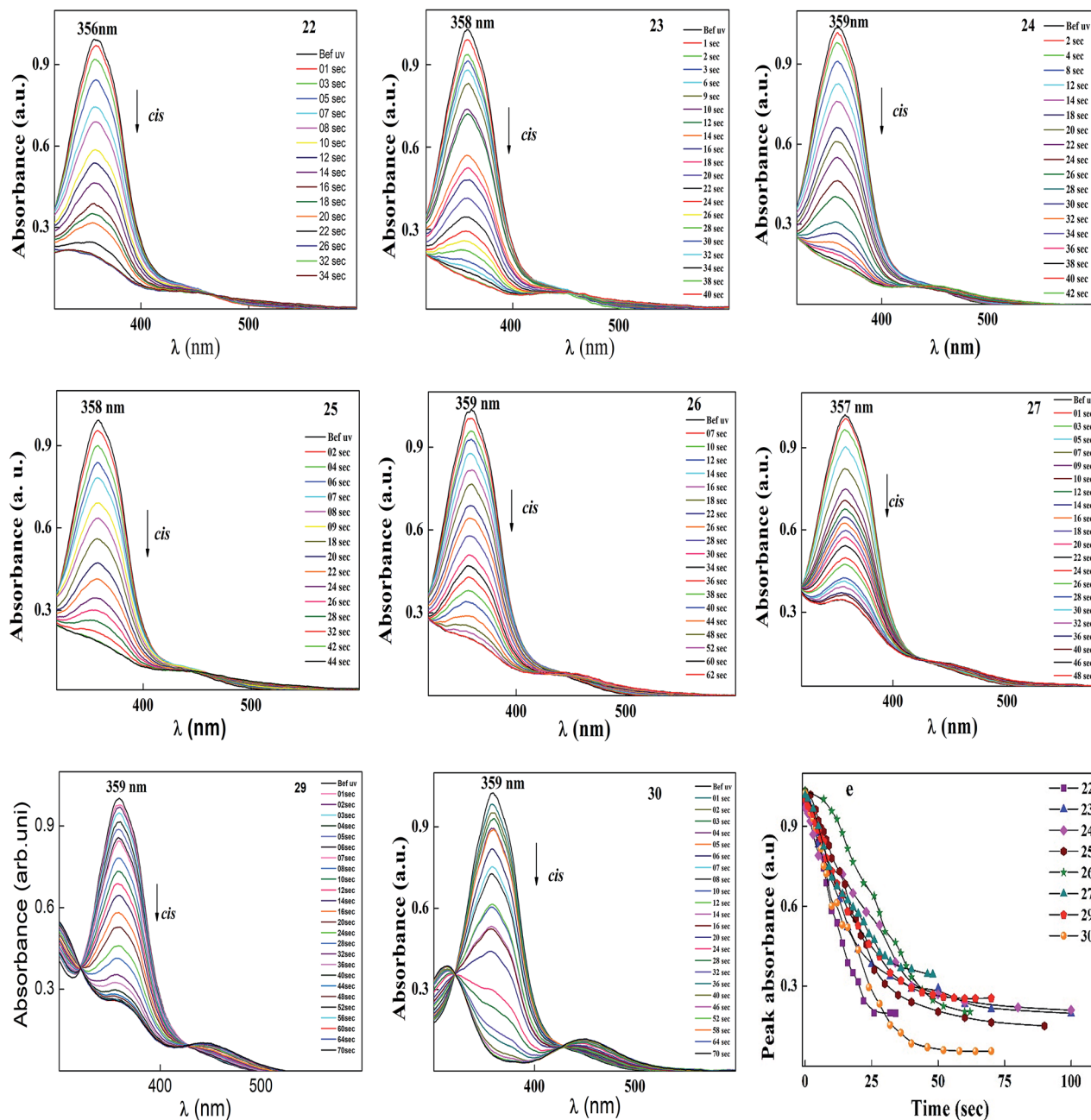


Fig. 11 Normalized absorption spectra of compounds 22–30 as a function of UV irradiation time. Graph (e) peak absorbance plot for *trans*–*cis* isomerization extracted from the absorption spectra (in this figure) of 22–30 upon UV illumination. Intensity of the UV light used was 1 mW cm^{-2} .

Table 6 The summarized data of *E/Z* isomerisation, thermal back relaxation and its photoconversion efficiency

Compound code	<i>E/Z</i> isomerization in s	Thermal back relaxation in min	CE %
22	25	60	80.20
23	32	160	80.64
24	46	210	77.42
25	32	140	85.43
26	48	240	80.33
27	36	270	66.18
29	44	390	74.55
30	46	590	94.43

The *E/Z* and *Z/E* photoisomerization behaviour of the solid cell is depicted in Fig. 15. The intensity used for achieving photosaturation was around 1.2 mW cm^{-2} and it took $\sim 80 \text{ s}$ to reach the photosaturation state (Fig. 15a and b). In contrast, back relaxation, which occurred in the absence of light, took around $\sim 400 \text{ min}$ to reach the original position (Fig. 15c and d).

To see the effect of thermal back relaxation, we fabricated an optical storage device with the above mixture. Previously prepared ITO coated, unidirectionally rubbed polyimide layers were sandwiched between two glass plates with a uniform thickness of $\sim 5 \mu\text{m}$. The device, as depicted in



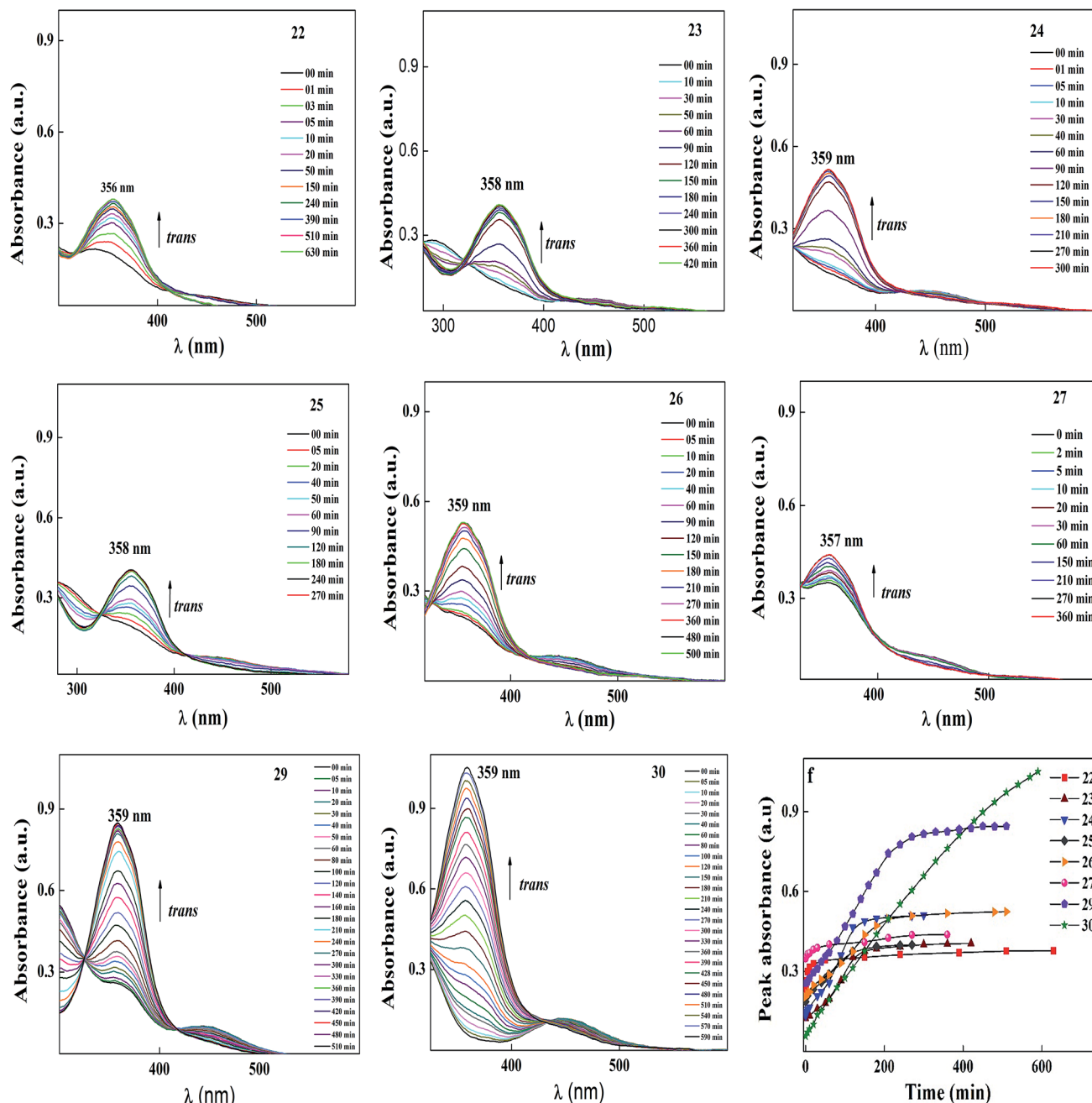


Fig. 12 Normalized absorption spectra of compounds 22–30 as a function of recovery time during thermal back relaxation. Graph (f) peak absorbance plot for *cis*–*trans* isomerization extracted from the absorption spectra (in this figure) of 22–30 during thermal back relaxation.

Fig. 16, showed bright and dark regions after illumination with UV light of intensity 1.2 mW cm^{-2} for 10 min using suitable masks. As can be seen from the figure, the exposed region where UV light is illuminated transforms from an ordered nematic state to a disordered isotropic state (black region), whereas the masked region remains in the nematic phase (bright region). To transfer back to the original nematic phase from the isotropic phase, the device took around 250 min, showing the potential of the optical rewriting capabilities of the materials.

2.7 Proposed model for guest–host effect

When UV light of 365 nm was illuminated on the composite mixture of azobenzene and liquid crystal molecules, the energetically stable *trans* isomer (order state) transformed to the *cis*-isomer (disorder state). The guest-host effect of azobenzene and liquid crystal molecules is schematically depicted Fig. 17, which shows that the reverse transformation of the *cis* isomer is not easy to reach its original state due to the presence of hydrophobic and hydrophilic head groups on the azo molecules.



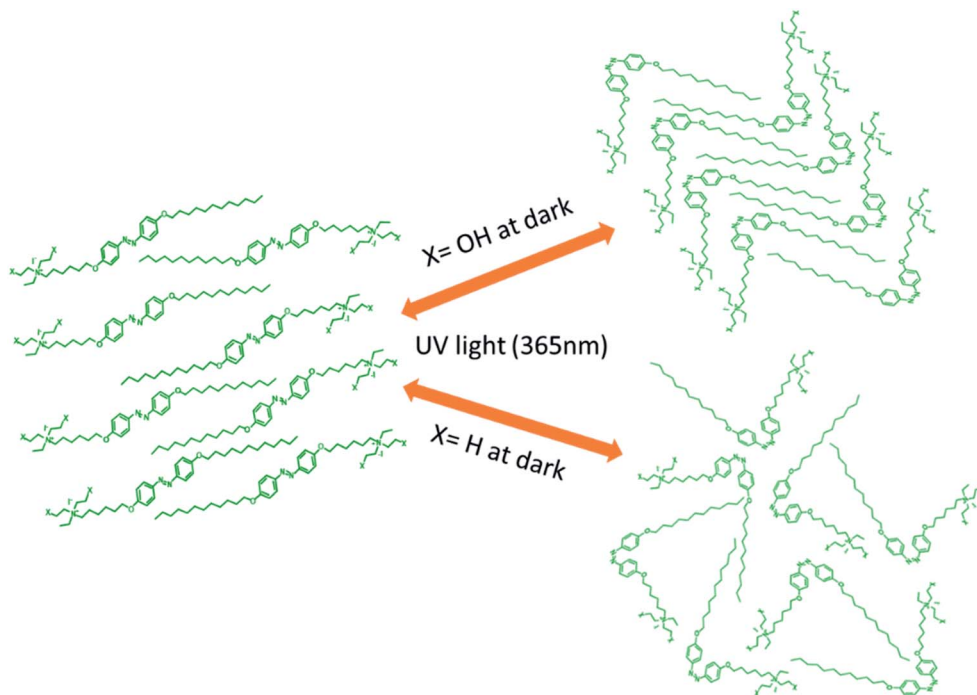


Fig. 13 Schematic diagram of the light-induced *trans*–*cis* isomerization of compounds 22–30 (if X = OH, layered order arrangements of molecules and if X = H, molecules are randomly arranged).

3 Experimental

3.1 Materials and methods

N,N-Dimethylethanolamine (99%), ethanol (99.9%), ethyl iodide (98%), 2-propanol (99%), HCl conc. (35%), NaNO₂ (99%), phenol (98%) K₂CO₃ (99.5%), Na₂CO₃ (99.5%), NaOH (98%), 1-bromododecane (99%), 1-bromoheptane (99%), 1-bromooctane (99%) and 1,6-dibromohexane (99%) were purchased from Acros Organics and used without further purification. Petroleum ether (b.p. 60–90 °C), acetonitrile (99.9%), dichloromethane (99.9%), acetone (99%) and ethyl acetate (99%) were commercial products obtained from Acros Organics. ¹H NMR (400 MHz) and ¹³C NMR (100 MHz) were recorded on a Bruker 400 MHz Ultrashield™ spectrometer. Elemental analysis was performed using a CHN elemental analyser.

3.1.1 General synthetic procedure for 4-acetamidophenox-yalkanes (1–3). To a 250 mL round-bottom flask containing 4-acetamidophenol (1.0 equiv.) in dry acetone, anhydrous potassium carbonate (3.0 equiv.), a catalytic amount of potassium iodide and the corresponding 1-bromoalkane (1.1 equiv.) were added. The reaction mixture was refluxed for 48 h. The reaction progress was monitored by TLC. After completion of the reaction, excess solvent was removed using a rotatory evaporator. The crude product was washed with distilled water to remove excess potassium carbonate and the residue was filtered and dried. Excess 1-bromoalkane was removed by washing the residue with *n*-hexane. The crude product was purified by column chromatography using ethyl acetate/hexane (v/v, 30 : 70) to yield compounds 1–3.

(1) (*n* = 7) yield: 71.5%. ¹H NMR (400 MHz, CDCl₃) δ/ppm 7.38–7.32 (m, 2H), 7.13 (s, 1H), 6.88–6.80 (m, 2H), 3.96–3.88

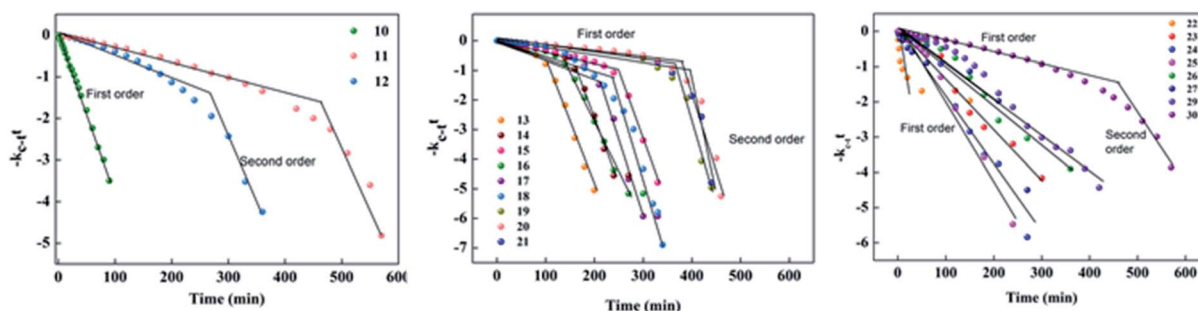


Fig. 14 First-order plot for the thermal back relaxation of compounds 10–30 measured at room temperature.



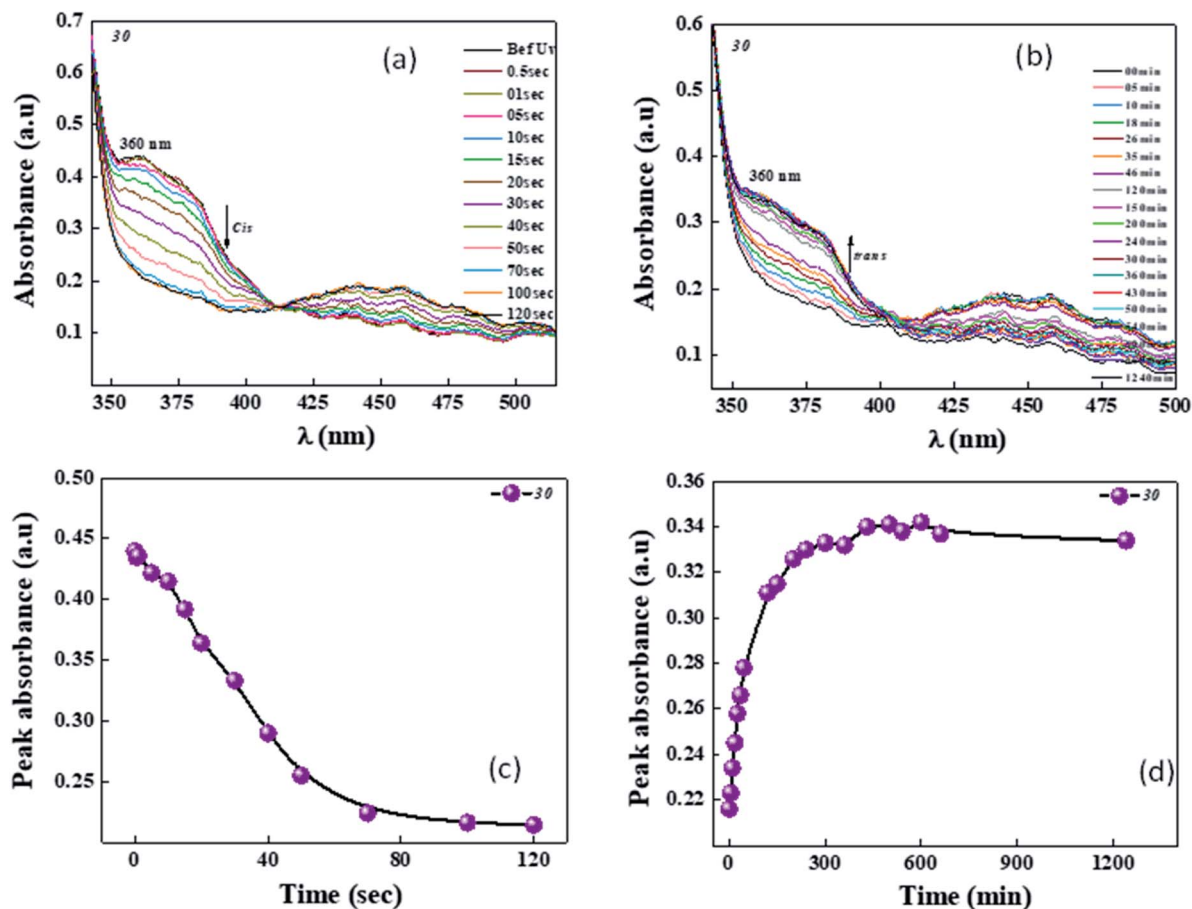


Fig. 15 E/Z (a and b) and Z/E (c and d) photoisomerization of the solid cell filled with the mixture of compound **30** and room temperature liquid crystals as guest–host combination. Intensity used was around 1.2 mW cm^{-2} , where the light-sensitive moiety (which is compound **30**) acts like the guest and MLC-6873-100, which is a room temperature liquid crystal, acts as the host.

(m, 2H), 2.14 (s, 3H), 1.80–1.69 (m, 2H), 1.43 (dt, $J = 15.1$, 6.6 Hz, 2H), 1.33 (ddd, $J = 15.0$, 8.6, 4.6 Hz, 6H), 0.88 (t, $J = 6.9$ Hz, 3H).

(2) ($n = 8$) yield: 68.82%. $^1\text{H NMR}$ (400 MHz, CDCl_3) δ /ppm 7.39–7.33 (m, 2H), 6.89–6.78 (m, 2H), 3.97–3.84 (m, 2H), 1.81–1.68 (m, 2H), 1.49–1.37 (m, 2H), 1.37–1.20 (m, 8H), 0.87 (t, $J = 6.9$ Hz, 3H).

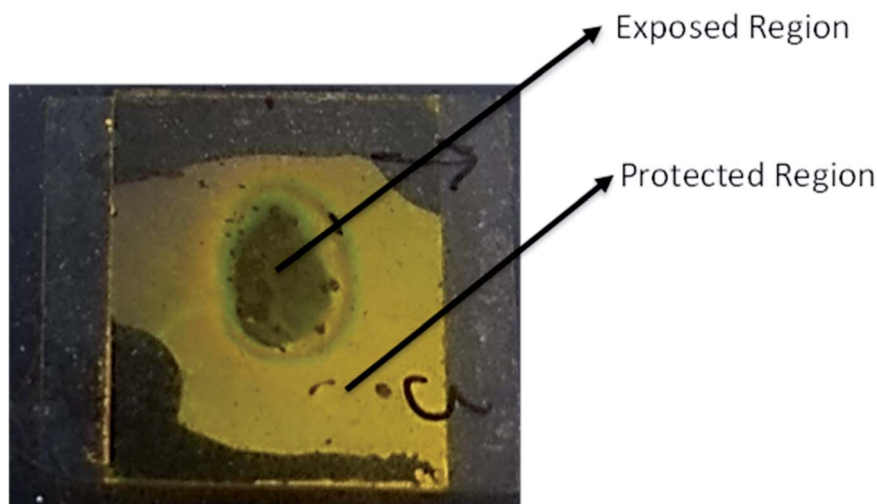


Fig. 16 Demonstration of the optical storage device described herein through UV illumination together with a photomask. Bright region corresponds to the non-illuminated area, whereas, the dark region corresponds to the UV illuminated area. Material transformed from the nematic to isotropic phase during illumination, showing excellent dark and bright states between them.



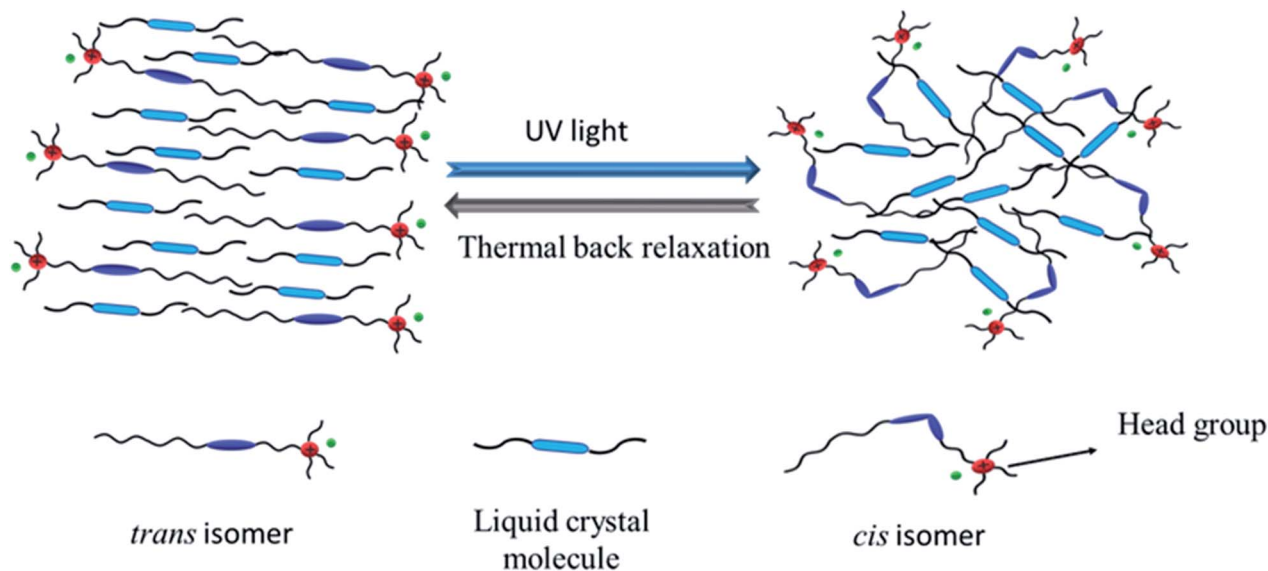


Fig. 17 Schematic diagram of the guest–host effect of the azobenzene-based ionic liquid and liquid crystal molecules.

(3) ($n = 12$) yield: 83.5% ^1H NMR (400 MHz, CDCl_3) δ/ppm 7.37–7.31 (m, 2H), 7.12 (s, 1H), 6.86–6.82 (m, 2H), 3.98–3.88 (m, 2H), 2.14 (s, 3H), 1.81–1.67 (m, 2H), 1.49–1.38 (m, 2H), 1.38–1.22 (m, 17H), 0.87 (t, $J = 6.9$ Hz, 3H).

3.1.2 General synthetic procedure for 4-alkoxyanilines (4–6). To a 250 mL round-bottom flask containing the corresponding 4-acetamidophenoxyalkanes (1–3), sodium hydroxide pellets in ethanol were added. The reaction mixture was refluxed for 24 h. The reaction progress was monitored by TLC. After completion of the reaction, the excess solvent was evaporated using a rotatory evaporator. The crude product was purified *via* recrystallization from ethanol.

(4) ($n = 7$) yield: ^1H NMR (400 MHz, CDCl_3) δ/ppm 6.76–6.69 (m, 2H), 6.66–6.58 (m, 2H), 4.06 (t, $J = 6.6$ Hz, 2H), 1.73 (m, 2H), 1.45–1.36 (m, 2H), 1.36–1.22 (m, 6H), 0.88 (t, $J = 6.9$ Hz, 3H).

(5) ($n = 8$) yield: 80%. ^1H NMR (400 MHz, CDCl_3) δ/ppm 6.76–6.70 (m, 2H), 6.65–6.60 (m, 2H), 4.04 (t, $J = 6.6$ Hz, 2H), 1.74 (m, 2H), 1.43 (m, 2H), 1.30–1.26 (m, 8H), 0.87 (t, $J = 6.9$ Hz, 3H).

(6) ($n = 12$) yield: 70%. ^1H NMR (400 MHz, CDCl_3) δ/ppm 6.76–6.70 (m, 2H), 6.65–6.59 (m, 2H), 4.06 (t, $J = 6.6$ Hz, 2H), 1.74 (m, 2H), 1.43 (m, 2H), 1.29–1.26 (m, 16H), 0.87 (t, $J = 6.9$ Hz, 3H).

3.1.3 General synthetic procedure for 4-[(4'-alkoxyphenyl)diazanyl]phenols, 7–9. In a 250 mL round-bottom flask, the corresponding 4-alkoxyanilines, 4–6 (1.0 equiv.) were dissolved in a mixture of acetone (100 mL) and concentrated hydrochloric acid. The reaction mixture was stirred for 1 h with the temperature of the mixture maintained below 0°C . A cold solution of phenol (1.0 equiv.), sodium hydroxide (1.0 equiv.) and sodium carbonate (1.0 equiv.) was then added dropwise to the reaction mixture and it was stirred for another hour at 0°C , thereafter the ice-water bath was removed, and it was stirred at room temperature overnight. The reaction mixture was then neutralized with an aqueous solution of sodium hydroxide, upon which a reddish-brown precipitate was formed. The

crude products were filtered, washed with distilled water and recrystallized from *n*-hexane to yield compounds 7–9.

(7) ($n = 7$) yield: ^1H NMR (400 MHz, CDCl_3) δ/ppm 7.87–7.77 (m, 4H), 7.01–6.85 (m, 4H), 4.02 (t, $J = 6.6$ Hz, 2H), 1.87–1.75 (m, 2H), 1.47 (dt, $J = 14.6, 6.7$ Hz, 2H), 1.40–1.23 (m, 6H), 0.89 (t, $J = 6.9$ Hz, 3H).

(8) ($n = 8$) yield: 47%. ^1H NMR (400 MHz, CDCl_3) δ/ppm 7.88–7.78 (m, 4H), 7.01–6.95 (m, 2H), 6.95–6.88 (m, 2H), 5.04 (s, 1H), 4.02 (t, $J = 6.6$ Hz, 2H), 1.86–1.74 (m, 2H), 1.51–1.41 (m, 2H), 1.41–1.22 (m, 8H), 0.88 (t, $J = 6.9$ Hz, 3H).

(9) ($n = 12$) yield: 73.5%. 400 MHz, CDCl_3) δ/ppm 7.87–7.79 (m, 2H), 7.00–6.96 (m, 1H), 6.95–6.91 (m, 1H), 4.02 (t, $J = 6.6$ Hz, 1H), 1.85–1.76 (m, 1H), 1.46 (dd, $J = 15.4, 7.0$ Hz, 1H), 1.26 (s, 9H), 0.87 (t, $J = 6.9$ Hz, 2H).

3.1.4 General synthetic procedure for *N*-[4-(bromohexyloxy)phenyl]-*N*-(alkoxyphenyl)diazenes, 10–12. To 250 mL a round-bottom flask containing 4-[(4'-alkoxyphenyl)diazanyl]phenols, 7–9 (1.0 equiv.) in dry acetone, 1,6-dibromohexane (7.0 equiv.), anhydrous potassium carbonate (3.0 equiv.) and a catalytic amount of potassium iodide were added. The reaction mixture was refluxed for 7 h. The reaction progress was monitored by TLC. After completion of the reaction, excess solvent was removed using a rotatory evaporator, upon which a yellow precipitate was formed. The crude product was washed with distilled water to remove excess potassium carbonate and the residue was filtered and dried. Excess 1,6-dibromohexane was removed by washing the residue with *n*-hexane and the products were recrystallized from methanol to yield compounds 10–12.

(10) ($n = 7$) yield: ^1H NMR (400 MHz, CDCl_3) δ/ppm 7.89–7.81 (m, 4H), 7.01–6.94 (m, 4H), 4.03 (td, $J = 6.5, 3.9$ Hz, 4H), 3.43 (t, $J = 6.8$ Hz, 2H), 1.95–1.85 (m, 3H), 1.86–1.75 (m, 4H), 1.50–1.41 (m, 2H), 1.33 (ddd, $J = 11.3, 10.4, 5.2$ Hz, 6H), 0.89 (dd, $J = 9.0, 4.8$ Hz, 3H).

(11) ($n = 8$) yield: 77.5%. ^1H NMR (400 MHz, CDCl_3) δ/ppm 7.88–7.82 (m, 4H), 6.98 (dd, $J = 9.0, 1.0$ Hz, 4H), 4.02 (td, $J = 6.5,$



4.5 Hz, 4H), 3.42 (q, $J = 6.4$ Hz, 2H), 1.90 (dd, $J = 13.9$, 7.0 Hz, 2H), 1.86–1.71 (m, 4H), 1.51 (dd, $J = 9.8$, 6.2 Hz, 3H), 1.48–1.40 (m, 2H), 1.26 (s, 16H), 0.87 (t, $J = 6.8$ Hz, 3H).

(12) ($n = 12$) yield: 50%. ^1H NMR (400 MHz, CDCl_3) δ /ppm 7.88–7.82 (m, 4H), 6.98 (dd, $J = 9.0$, 1.0 Hz, 4H), 4.02 (td, $J = 6.5$, 4.5 Hz, 4H), 3.42 (q, $J = 6.4$ Hz, 2H), 1.90 (dd, $J = 13.9$, 7.0 Hz, 2H), 1.86–1.71 (m, 4H), 1.51 (dd, $J = 9.8$, 6.2 Hz, 3H), 1.48–1.40 (m, 2H), 1.26 (s, 16H), 0.87 (t, $J = 6.8$ Hz, 3H).

3.1.5 General synthetic procedure for *N,N*-diethanol-6-(4-((4'-alkyloxyphenyl)diazinyl)phenoxy)hexan-1-amines, 13–15. To a 250 mL round-bottom flask containing the corresponding *N*-[4-(bromohexyloxy)phenyl]-*N*-(alkyloxyphenyl)diazenes, 10–12, in 2-propanol, *N,N*-diethanol amine was added in excess. The reaction mixture was refluxed for 38 h. The reaction progress was monitored by TLC. After completion of the reaction, excess solvent was removed using a rotatory evaporator. The crude products were recrystallized from ethanol to yield compounds 13–15.

(13) ($n = 7$) yield: 73.02%. ^1H NMR (400 MHz, CDCl_3) δ /ppm 7.87–7.81 (m, 4H), 6.98 (t, $J = 5.9$ Hz, 4H), 4.05–3.98 (m, 4H), 3.66–3.57 (m, 4H), 2.66 (t, $J = 5.4$ Hz, 4H), 2.57–2.50 (m, 2H), 1.86–1.74 (m, 6H), 1.56–1.42 (m, 6H), 1.42–1.20 (m, 9H), 0.88 (q, $J = 7.0$ Hz, 3H).

(14) ($n = 8$) yield: 73.8%. ^1H NMR (400 MHz, CDCl_3) δ /ppm 7.88–7.81 (m, 4H), 6.98 (t, $J = 6.0$ Hz, 4H), 4.05–3.99 (m, 4H), 3.62 (t, $J = 5.4$ Hz, 4H), 2.67 (t, $J = 5.4$ Hz, 4H), 2.54 (d, $J = 7.5$ Hz, 2H), 1.80 (dt, $J = 14.6$, 5.2 Hz, 5H), 1.49 (dd, $J = 13.5$, 6.4 Hz, 6H), 1.41–1.23 (m, 11H), 0.88 (t, $J = 6.9$ Hz, 3H).

(15) ($n = 12$) yield: 52.6%. ^1H NMR (400 MHz, CDCl_3) δ /ppm 7.87–7.82 (m, 4H), 6.98 (d, $J = 9.0$ Hz, 4H), 4.02 (td, $J = 6.5$, 1.9 Hz, 4H), 3.62 (td, $J = 5.4$, 2.9 Hz, 4H), 2.66 (dd, $J = 9.8$, 4.5 Hz, 4H), 2.57–2.51 (m, 2H), 1.80 (dd, $J = 16.8$, 9.0 Hz, 7H), 1.55–1.41 (m, 7H), 1.36 (dd, $J = 20.2$, 11.4 Hz, 5H), 1.26 (s, 15H), 0.86 (d, $J = 7.0$ Hz, 3H).

3.1.6 General synthetic procedure for *N*-ethyl-*N*-ethanol-6-(4-((4'-alkyloxyphenyl)diazinyl)phenoxy)hexan-1-amines, 16–18. To a 250 mL round-bottom flask containing the corresponding *N*-[4-(bromohexyloxy)phenyl]-*N*-(alkyloxyphenyl)diazenes, 10–12 in 2-propanol, *N*-ethyl-*N*-ethanol amine was added in excess. The reaction mixture was refluxed for 38 h and the reaction progress was monitored by TLC. After completion of the reaction, excess solvent was removed using a rotatory evaporator. The crude products were recrystallized from ethanol to yield compounds 16–18.

(16) ($n = 7$) yield: 64.6%. ^1H NMR (400 MHz, CDCl_3) δ /ppm 7.86–7.81 (m, 4H), 6.98 (dd, $J = 6.9$, 5.0 Hz, 4H), 4.02 (t, $J = 6.6$ Hz, 4H), 3.55–3.51 (m, 2H), 2.60–2.52 (m, 4H), 2.49–2.44 (m, 2H), 1.85–1.77 (m, 4H), 1.53–1.41 (m, 7H), 1.42–1.25 (m, 10H), 1.04–0.99 (m, 3H), 0.90–0.85 (m, 3H).

(17) ($n = 8$) yield: 52.9%. ^1H NMR (400 MHz, CDCl_3) δ /ppm 7.84 (t, $J = 9.0$ Hz, 4H), 6.96 (t, $J = 9.0$ Hz, 4H), 4.02 (t, $J = 6.2$ Hz, 4H), 3.53 (t, $J = 5.4$ Hz, 2H), 2.61–2.51 (m, 4H), 2.49–2.43 (m, 2H), 1.86–1.76 (m, 4H), 1.54–1.42 (m, 6H), 1.41–1.23 (m, 10H), 1.01 (t, $J = 7.1$ Hz, 3H), 0.88 (t, $J = 6.8$ Hz, 3H).

(18) ($n = 9$) yield: 61.3%. ^1H NMR (400 MHz, CHLOROFORM-D) δ 7.88–7.82 (m, 15H), 7.01–6.95 (m, 15H), 4.06–3.99 (m, 15H), 3.53 (t, $J = 5.4$ Hz, 8H), 2.60–2.52 (m, 17H), 2.49–2.44 (m, 8H),

1.81 (dd, $J = 13.2$, 6.1 Hz, 16H), 1.53–1.42 (m, 26H), 1.42–1.33 (m, 17H), 1.26 (s, 52H), 1.05–0.98 (m, 11H), 0.87 (t, $J = 6.9$ Hz, 11H).

3.1.7 *N,N*-diethyl-6-(4-((4'-alkyloxyphenyl)diazinyl)phenoxy)hexan-1-amines, 19–21. To a 250 mL round-bottom flask containing the corresponding *N*-[4-(bromohexyloxy)phenyl]-*N*-(alkyloxyphenyl)diazenes, 10–12, in 2-propanol, *N,N*-diethyl amine was added in excess. The reaction mixture was refluxed for 38 h and the reaction progress was monitored by TLC. After completion of the reaction, excess solvent was removed using a rotatory evaporator. The crude products were recrystallized from ethanol to yield compounds 19–21.

(19) ($n = 7$) yield: 60%. ^1H NMR (400 MHz, CDCl_3) δ /ppm 7.88–7.82 (m, 4H), 7.00–6.95 (m, 4H), 4.02 (t, $J = 6.5$ Hz, 4H), 2.53 (q, $J = 7.1$ Hz, 4H), 2.46–2.40 (m, 2H), 1.80 (dt, $J = 14.9$, 5.5 Hz, 4H), 1.49 (dd, $J = 12.9$, 5.5 Hz, 7H), 1.41–1.27 (m, 9H), 1.02 (t, $J = 7.2$ Hz, 6H), 0.89 (t, $J = 6.9$ Hz, 3H).

(20) ($n = 8$) yield: 93.5%. 7.86–7.82 (m, 4H), 7.00–6.93 (m, 4H), 4.01 (t, $J = 6.5$ Hz, 4H), 2.52 (q, $J = 7.1$ Hz, 4H), 2.44–2.40 (m, 2H), 1.78 (dt, $J = 14.9$, 5.5 Hz, 4H), 1.47 (dd, $J = 12.9$, 5.5 Hz, 10H), 1.41–1.27 (m, 10H), 1.02 (t, $J = 7.2$ Hz, 6H), 0.89 (t, $J = 6.9$ Hz, 3H).

(21) ($n = 12$) yield: 85.71%. ^1H NMR (400 MHz, CDCl_3) δ /ppm 7.85 (d, $J = 8.9$ Hz, 4H), 6.97 (d, $J = 9.1$ Hz, 4H), 4.02 (t, $J = 5.9$ Hz, 4H), 2.52 (dd, $J = 14.4$, 7.2 Hz, 4H), 2.45–2.39 (m, 2H), 1.81 (dd, $J = 13.6$, 7.0 Hz, 5H), 1.53–1.43 (m, 7H), 1.31 (d, $J = 40.8$ Hz, 20H), 1.02 (t, $J = 7.2$ Hz, 6H), 0.87 (t, $J = 6.7$ Hz, 3H).

3.1.8 *N,N*-diethanol-6-(4-((4'-alkyloxyphenyl)diazinyl)phenoxy)hexan-1-ammonium iodides, 22–24. To a 250 mL round-bottom flask containing the corresponding *N,N*-diethanol-6-(4-((4'-alkyloxyphenyl)diazinyl)phenoxy)hexan-1-amines in acetonitrile, 13–15, excess ethyl iodide was added. The reaction mixture was refluxed for 36 h and the reaction progress was monitored by TLC. After completion of the reaction, excess solvent was removed using a rotatory evaporator. The crude product was recrystallized from a mixture of ethanol/*n*-hexane to yield compounds 22–24.

(22) ($n = 7$) yield: 30.8%. Elemental analysis: calculated for $\text{C}_{31}\text{H}_{50}\text{IN}_3\text{O}_4$: C = 56.79, H = 7.69, N = 6.41; found: C = 56.184, H = 7.601, N = 6.327. HRMS $[\text{C}_{31}\text{H}_{50}\text{N}_3\text{O}_4]^+ = 528.3802$. ^1H NMR (400 MHz, CDCl_3) δ /ppm 7.86–7.81 (m, 16H), 6.97 (ddd, $J = 6.9$, 5.0, 2.6 Hz, 16H), 4.10 (s, 16H), 4.05–3.98 (m, 25H), 3.68–3.63 (m, 15H), 3.57 (q, $J = 7.1$ Hz, 8H), 3.48–3.41 (m, 8H), 1.80 (dt, $J = 8.0$, 6.5 Hz, 17H), 1.60–1.51 (m, 10H), 1.50–1.39 (m, 18H), 1.39–1.25 (m, 40H), 0.90–0.86 (m, 12H). ^{13}C NMR (101 MHz, CDCl_3) δ /ppm 161.34, 161.07, 146.94, 124.74 (d, $J = 8.0$ Hz), 124.41, 124.04, 123.71, 115.06–114.54, 114.40 (d, $J = 8.1$ Hz), 110.98 (d, $J = 1.4$ Hz), 103.65 (s), 89.59 (d, $J = 3.2$ Hz), 83.33 (d, $J = 12.1$ Hz), 82.92 (s), 82.53 (s), 82.15 (s), 82.03–81.83, 81.60, 81.37–81.16, 80.95 (dd, $J = 14.1$, 9.8 Hz), 80.71, 80.24 (d, $J = 7.7$ Hz), 79.85 (dd, $J = 16.6$, 7.4 Hz), 79.09 (s), 78.86–77.71 (m), 77.73–77.71 (m), 77.38 (d, $J = 11.9$ Hz), 77.12, 76.41 (d, $J = 77.7$ Hz), 75.09 (d, $J = 17.3$ Hz), 74.72, 74.61–74.09, 73.87–73.45, 73.30 (d, $J = 6.8$ Hz), 72.84 (s), 71.45 (s), 68.48 (d, $J = 10.6$ Hz), 67.97 (d, $J = 13.3$ Hz), 66.34 (s), 65.04 (d, $J = 14.4$ Hz), 60.69 (d, $J = 7.2$ Hz), 59.93 (s), 56.00 (s), 55.53 (d, $J = 17.3$ Hz), 53.69–53.28, 41.42 (d, $J = 1.4$ Hz), 40.45 (d, $J = 5.3$ Hz), 39.54–39.25, 32.31–31.75, 31.12 (d, $J = 19.6$ Hz), 29.75, 29.50–28.77, 26.37–25.47,



24.73, 22.85–22.45, 21.88 (d, $J = 52.8$ Hz), 14.56, 14.17, 8.41 (d, $J = 11.6$ Hz), 4.12 (dd, $J = 28.5$, 9.0 Hz), –20.92 to –21.26.

(23) ($n = 8$) yield: 40.0%. Elemental analysis: calculated for $C_{32}H_{52}IN_3O_4$: C = 57.39, H = 7.83, N = 6.27; found: C = 57.019, H = 7.707, N = 6.175. HRMS $[C_{32}H_{52}N_3O_4]^+ = 542.3959$. 1H NMR (400 MHz, $CDCl_3$) δ /ppm 7.84 (d, $J = 8.9$ Hz, 6H), 7.00–6.94 (m, 6H), 4.10 (s, 8H), 4.01 (q, $J = 6.5$ Hz, 6H), 3.66 (s, 6H), 3.57 (dd, $J = 14.2$, 6.9 Hz, 3H), 3.48–3.41 (m, 4H), 1.80 (dd, $J = 14.2$, 7.1 Hz, 6H), 1.76–1.70 (m, 4H), 1.55 (d, $J = 7.2$ Hz, 4H), 1.45 (d, $J = 7.2$ Hz, 7H), 1.32 (dd, $J = 18.5$, 11.3 Hz, 17H), 0.87 (dd, $J = 9.2$, 4.5 Hz, 4H). ^{13}C NMR (101 MHz, $CDCl_3$) δ /ppm 161.35 (s), 161.08 (s), 146.93 (d, $J = 13.1$ Hz), 124.42 (s), 114.82 (d, $J = 11.1$ Hz), 77.45 (s), 77.13 (s), 76.81 (s), 68.43 (s), 68.04 (s), 60.64 (s), 59.94 (s), 56.00 (s), 55.60 (s), 31.90 (s), 29.55–29.20 (m), 29.03 (s), 26.10 (s), 25.67 (s), 22.69 (d, $J = 10.1$ Hz), 22.15 (s), 14.20 (s), 8.49 (s).

(24) ($n = 12$) yield: 36.8%. Elemental analysis: calculated for $C_{36}H_{60}IN_3O_4$: C = 59.58, H = 8.33, N = 5.79; found: C = 59.39, H = 8.25, N = 5.709. HRMS $[C_{36}H_{60}N_3O_4]^+ = 598.4585$. 1H NMR (400 MHz, $CDCl_3$) δ /ppm 7.84 (dd, $J = 9.0$, 0.7 Hz, 16H), 7.00–6.94 (m, 16H), 4.11 (s, 16H), 4.01 (dd, $J = 14.2$, 6.5 Hz, 20H), 3.67 (d, $J = 3.1$ Hz, 15H), 3.58 (q, $J = 7.2$ Hz, 8H), 3.49–3.42 (m, 8H), 1.86–1.76 (m, 17H), 1.72 (dd, $J = 16.3$, 9.4 Hz, 10H), 1.45 (dt, $J = 14.1$, 7.2 Hz, 19H), 1.34 (t, $J = 7.2$ Hz, 25H), 1.27 (d, $J = 13.8$ Hz, 57H), 0.87 (t, $J = 6.9$ Hz, 12H). ^{13}C NMR (101 MHz, $CDCl_3$) δ /ppm 161.35, 161.05, 146.97 (d, $J = 14.8$ Hz), 124.4, 114.81 (d, $J = 9.0$ Hz), 77.43, 77.11, 76.79, 68.43, 67.98, 60.69, 59.96, 55.97, 55.68, 53.52, 32.00, 31.02, 29.86–29.17, 29.02, 26.11, 25.69, 22.77, 22.15, 14.21, 8.39.

3.1.9 *N*-ethyl-*N*-ethanol-6-(4-((4'-alkyloxyphenyl)diazenyl)phenoxy)hexan-1-ammonium iodides, 25–27. Compounds 25–17 were synthesized following the procedure described for the preparation of compounds 22–24, using the corresponding *N*-ethyl-*N*-ethanol-6-(4-((4'-alkyloxyphenyl)diazenyl)phenoxy)hexan-1-amines 16–18 as the starting materials.

(25) ($n = 7$) yield: 60.0%. Elemental analysis: calculated for $C_{31}H_{50}IN_3O_3$: C = 58.21, H = 7.88, N = 6.57; found: C = 57.724, H = 7.802, N = 6.302. HRMS $[C_{31}H_{50}N_3O_3]^+ = 512.3839$. 1H NMR (400 MHz, $CDCl_3$) δ /ppm 7.84 (dd, $J = 9.0$, 0.7 Hz, 4H), 7.01–6.94 (m, 4H), 4.36 (t, $J = 6.0$ Hz, 1H), 4.12 (s, 2H), 4.02 (dt, $J = 9.4$, 6.4 Hz, 4H), 3.58–3.47 (m, 6H), 3.43–3.36 (m, 2H), 1.88–1.70 (m, 6H), 1.63–1.53 (m, 4H), 1.47 (td, $J = 14.3$, 7.1 Hz, 4H), 1.36 (t, $J = 7.1$ Hz, 7H), 1.33–1.27 (m, 4H), 0.89 (t, $J = 6.9$ Hz, 3H). ^{13}C NMR (101 MHz, $CDCl_3$) δ /ppm 161.34, 161.06, 146.96 (d, $J = 12.7$ Hz), 124.40, 114.81 (d, $J = 7.5$ Hz), 100.00, 77.48, 77.16, 76.84, 75.37, 68.43, 67.97, 59.56, 58.88, 55.35, 54.80, 31.85, 29.15 (t, $J = 13.9$ Hz), 26.12 (d, $J = 12.5$ Hz), 25.70, 22.64 (d, $J = 7.9$ Hz), 22.21, 14.17, 8.37.

(26) ($n = 8$) yield: 62.5%. Elemental analysis: calculated for $C_{31}H_{50}IN_3O_4$: C = 58.80, H = 8.02, N = 6.43; found: C = 58.435, H = 7.919, N = 6.287. HRMS $[C_{32}H_{52}N_3O_3]^+ = 526.4027$. Yield: 1H NMR (400 MHz, $CDCl_3$) δ /ppm 7.84 (d, $J = 8.7$ Hz, 4H), 6.97 (dd, $J = 9.0$, 2.2 Hz, 4H), 4.36 (t, $J = 6.0$ Hz, 1H), 4.12 (s, 2H), 4.02 (dt, $J = 9.6$, 6.4 Hz, 4H), 3.55 (d, $J = 8.7$ Hz, 2H), 3.53–3.45 (m, 3H), 3.43–3.34 (m, 2H), 1.89–1.68 (m, 6H), 1.60–1.53 (m, 2H), 1.53–1.41 (m, 4H), 1.35 (t, $J = 7.2$ Hz, 7H), 1.29 (d, $J = 9.4$ Hz, 5H), 0.88 (t, $J = 6.8$ Hz, 3H). ^{13}C NMR (101 MHz, $CDCl_3$) δ /ppm 161.35 (d, $J = 2.4$ Hz), 161.07 (s), 146.92 (d, $J = 11.9$ Hz), 124.72–124.08, 122.78 (d, $J = 14.1$ Hz), 114.66 (dd, $J = 29.2$, 10.1 Hz),

77.47 (d, $J = 11.1$ Hz), 77.21, 76.89, 68.43, 68.00, 59.51, 58.85, 55.33, 54.81, 32.01–31.67, 29.55–29.18, 29.01, 26.35–25.94, 25.67, 22.87–22.57 (m), 22.19, 14.18, 8.41.

(27) ($n = 12$) yield: 20.8%. Elemental analysis: calculated for $C_{36}H_{60}IN_3O_3$: C = 60.92, H = 8.52, N = 5.92; found: C = 58.221, H = 8.095, N = 5.558. HRMS $[C_{36}H_{60}N_3O_3]^+ = 582.4630$. 1H NMR (400 MHz, $CDCl_3$) δ /ppm 7.84 (dd, $J = 8.9$, 0.7 Hz, 9H), 7.00–6.94 (m, 9H), 4.26 (t, $J = 5.8$ Hz, 2H), 4.14 (s, 4H), 4.03 (tt, $J = 11.3$, 5.9 Hz, 10H), 3.58–3.45 (m, 12H), 3.42–3.34 (m, 4H), 1.87–1.69 (m, 14H), 1.53–1.40 (m, 12H), 1.35 (t, $J = 7.2$ Hz, 17H), 1.32–1.19 (m, 36H), 0.86 (t, $J = 6.8$ Hz, 7H).

3.1.10 *N,N*-diethyl-6-(4-((4'-alkyloxyphenyl)diazenyl)phenoxy)hexan-1-ammonium iodides, 28–30. Compounds 28–30 were synthesized following the procedure described for the preparation of compounds 22–24 using the corresponding *N,N*-diethyl-6-(4-((4'-alkyloxyphenyl)diazenyl)phenoxy)hexan-1-amines 19–21 as the starting materials.

(28) ($n = 7$) yield: 15.0%. Elemental analysis: calculated for $C_{31}H_{50}IN_3O_2$: C = 59.70, H = 8.08, N = 6.74; found: C = 58.677, H = 7.889, N = 6.432. HRMS $[C_{31}H_{50}N_3O_2]^+ = 496.3918$. 1H NMR (400 MHz, $CDCl_3$) δ /ppm 7.85 (d, $J = 8.8$ Hz, 7H), 6.97 (d, $J = 8.9$ Hz, 7H), 4.08–3.99 (m, 7H), 3.45 (q, $J = 7.3$ Hz, 10H), 3.33–3.27 (m, 4H), 1.89–1.71 (m, 11H), 1.59 (s, 19H), 1.55–1.49 (m, 4H), 1.45 (dd, $J = 15.3$, 7.5 Hz, 4H), 1.39 (t, $J = 7.2$ Hz, 16H), 1.31 (s, 7H), 0.89 (t, $J = 6.9$ Hz, 5H). ^{13}C NMR (101 MHz, $CDCl_3$) δ /ppm 161.34 (s), 161.03 (s), 146.99 (d, $J = 13.7$ Hz), 124.41 (s), 114.80 (d, $J = 5.7$ Hz), 77.45 (s), 77.13 (s), 76.81 (s), 68.44 (s), 67.94 (s), 53.91 (s), 31.85 (s), 29.39–28.87 (m), 26.29 (s), 26.06 (s), 25.77 (s), 22.65 (d, $J = 7.1$ Hz), 22.31 (s), 14.18 (s), 8.44 (s).

(29) ($n = 8$) yield: 48.0%. Elemental analysis: calculated for $C_{32}H_{52}IN_3O_2$: C = 60.27, H = 8.22, N = 6.59; found: C = 59.338, H = 8.039, N = 6.273. HRMS $[C_{32}H_{52}N_3O_2]^+ = 510.4064$. 1H NMR (400 MHz, $CDCl_3$) δ /ppm 7.84 (d, $J = 8.5$ Hz, 8H), 6.97 (dd, $J = 9.0$, 1.3 Hz, 8H), 4.02 (dt, $J = 13.0$, 6.4 Hz, 8H), 3.44 (q, $J = 7.3$ Hz, 11H), 3.33–3.26 (m, 4H), 1.88–1.71 (m, 12H), 1.70–1.55 (m, 13H), 1.55–1.41 (m, 9H), 1.38 (t, $J = 7.2$ Hz, 17H), 1.30 (dt, $J = 16.8$, 10.5 Hz, 14H), 0.88 (dd, $J = 8.6$, 5.2 Hz, 6H). ^{13}C NMR (101 MHz, $CDCl_3$) δ /ppm 161.33, 161.03, 146.97 (d, $J = 12.8$ Hz), 124.39, 114.80 (d, $J = 5.8$ Hz), 77.47, 77.15, 76.83, 68.44, 67.95, 57.81, 53.88, 31.88, 29.37 (d, $J = 12.8$ Hz), 29.01, 26.19 (d, $J = 17.3$ Hz), 25.75, 22.73, 22.30, 14.19, 8.43.

(30) ($n = 12$) yield: 43.2%. Elemental analysis: calculated for $C_{36}H_{60}IN_3O_2$: C = 62.32, H = 8.72, N = 6.06; found: C = 61.73, H = 8.617, N = 5.913. HRMS $[C_{36}H_{60}N_3O_2]^+ = 566.4680$. 1H NMR (400 MHz, $CDCl_3$) δ /ppm 7.84 (d, $J = 8.6$ Hz, 4H), 6.97 (dd, $J = 8.9$, 1.5 Hz, 4H), 4.08–3.98 (m, 4H), 3.44 (q, $J = 7.2$ Hz, 6H), 3.33–3.26 (m, 2H), 1.89–1.71 (m, 6H), 1.57–1.49 (m, 3H), 1.49–1.43 (m, 2H), 1.38 (t, $J = 7.1$ Hz, 10H), 1.25 (s, 15H), 0.87 (t, $J = 6.7$ Hz, 3H). ^{13}C NMR (101 MHz, $CDCl_3$) δ /ppm 161.34, 161.04, 146.96 (d, $J = 12.8$ Hz), 124.39, 114.81 (d, $J = 7.0$ Hz), 77.48, 77.16, 76.84, 68.45, 67.98, 57.80, 53.88, 31.99, 30.02–29.18 (m), 29.02, 26.19 (d, $J = 19.0$ Hz), 25.76, 22.76, 22.28, 14.20, 8.43.

3.2 Mesomorphic studies

The thermal behaviour and liquid crystalline properties of all the synthesized compounds were studied *via* polarizing optical



microscopy (POM) and differential scanning calorimetry (DSC). For polarizing microscopy, a Linkam hot stage and temperature observation under polarized light of an Olympus BX 51 polarizing optical microscope were used. The magnification used to capture the optical texture was $10\times$ and $200\ \mu\text{m}$. DSC thermograms were recorded using a PerkinElmer DSC-7 with heating and cooling rates of $5\ ^\circ\text{C min}^{-1}$.

3.3 Photoswitching studies

The UV-vis spectra of the azobenzene-based ionic liquids and their intermediates were recorded using an Ocean Optics HR-2000+ UV-vis spectrophotometer setup. The photoisomerization of the azo compounds were recorded in a dark room in the wavelength range of 250 nm to 800 nm, and chloroform was used as the blank. At fixed concentration of $\sim 1.0 \times 10^{-5}\ \text{mol L}^{-1}$ of solution was prepared in chloroform and irradiated with a UV light source (Omni cure series 2000). The irradiation wavelength was 360 nm and a heat filter was used to keep heat radiation away from the source. The intensity of the irradiation light was $1\ \text{mW cm}^{-2}$, which was measured using a UV513AB UV meter. The absorption spectra of compounds **10–30** were recorded before illumination and after illumination. After reaching the photosaturation state, the thermal back relaxation was recorded by keeping the samples in the dark. For *trans-cis-trans* photoisomerization, the changes in absorption spectra upon UV illumination and thermal back relaxation were investigated with respect to time. For thermal back relaxation, first-order plots were plotted for *cis* (*Z*)-*trans* (*E*) isomerisation of all the compounds and measured at room temperature at $\sim 27\ ^\circ\text{C}$.

4 Conclusions

In summary, the photoresponsive behaviour of *N,N*-diethanol-6-(4-((4'-alkyloxyphenyl)diazanyl)phenoxy)hexan-1-ammonium iodides, **22–24**, *N*-ethyl-*N*-ethanol-6-(4-((4'-alkyloxyphenyl)diazanyl)phenoxy)hexan-1-ammonium iodides, **25–27** and *N,N*-diethyl-6-(4-((4'-alkyloxyphenyl)diazanyl)phenoxy)hexan-1-ammonium iodides, **28–30** and their intermediates **10–21** was characterized and their mesomorphic and photoswitching properties investigated. The schlieren texture of the smectic C (tilted) and smectic B phases was observed in case of the highest substituted carbon atom length in the alkoxy chain ($n = 12$) in the side chain of the azo moiety. The natural focal conic texture of the smectic A (non-tilted) phases was observed for all the compounds except the compound without a hydroxyl group in the terminal head group of its azo moieties. In the case of compound **30**, after 45 s, the photoequilibrium state was achieved under UV irradiation and its photoisomerization efficiency was greater than 95%. Its thermal back relaxation time was about ~ 590 min in solution at room temperature. The photoisomerization reaction rate was affected by the hydrophobic and hydrophilic head groups, and it also affected the equilibrium isomerization efficiency of the compounds. Thus, the azobenzene at the end of the head group bearing a hydroxyl group influences the thermal back

relaxation. As a result, the presence of a hydroxyl group on the ammonium group decreases the thermal back relaxation time. In the case of the solid cell, the thermal back relaxation time achieved was ~ 400 min. These results suggest that chemical modification of the photoresponsive behaviour of azobenzene derivatives can be useful for the design of molecular switches and optical storage devices.

Conflicts of interest

There are no conflicts to declare.

Acknowledgements

This research work was supported by DST-SERB (Department of Science and Technology-Science and Engineering Research Board) Govt of India under ECR grant (File No. ECR/2015/000190) and Universiti Sains Malaysia through the RUI research grant (Grant No. 1001/PKIMIA/8011094). We also thank Hima S Reddy for helping us to conduct the photoisomerization experiments.

Notes and references

- G. Hegde, G. Shankar, S. M. Gan, A. R. Yuvaraj, S. Mahmood and U. K. Mandal, *Liq. Cryst.*, 2016, **43**(11), 1578–1588.
- M. L. Rahman, M. M. Yusoff and S. Kumar, *RSC Adv.*, 2014, **4**(66), 35089–35098.
- M. L. Rahman, G. Hegde, M. Azazpour, M. M. Yusoff and S. Kumar, *J. Fluorine Chem.*, 2013, **156**, 230–235.
- L. Rahman, S. Kumar, C. Tschierske, G. Israel, D. Ster and G. Hegde, *Liq. Cryst.*, 2009, **36**(4), 397–407.
- M. R. Lutfor, G. Hegde, S. Kumar, C. Tschierske and V. G. Chigrinov, *Opt. Mater.*, 2009, **32**(1), 176–183.
- S. K. Prasad, G. G. Nair and D. S. Rao, *Liq. Cryst.*, 2009, **36**(6–7), 705–716.
- J. Sun and V. Chigrinov, *Mol. Cryst. Liq. Cryst.*, 2012, **561**(1), 1–7.
- M. R. Lutfor, M. M. Yusoff, G. Hegde, M. N. Fazli, A. Malek, N. A. Samah and H. T. Srinivasa, *Mol. Cryst. Liq. Cryst.*, 2013, **587**, 41–53.
- A. R. Yuvraj, W. S. Yam, T. N. Chan, Y. P. Goh and G. Hegde, *Spectrochim. Acta, Part A*, 2015, **135**, 1115–1122.
- Y. Norikane, Y. Hirai and M. Yoshida, *Chem. Commun.*, 2011, **47**(6), 1770–1772.
- A. Ziegler, J. Stumpe, A. Toutianoush and B. Tieke, *Colloids Surf., A*, 2002, **198**, 777–784.
- A. R. Yuvaraj, G. S. Mei, A. D. Kulkarni, M. Y. Mashitah and G. Hegde, *RSC Adv.*, 2014, **4**(92), 50811–50818.
- S. M. Gan, A. R. Yuvaraj, M. R. Lutfor, M. Y. Mashitah and H. Gurumurthy, *RSC Adv.*, 2015, **5**(9), 6279–6285.
- G. Hegde, V. M. Kozenkov, V. G. Chigrinov and H. S. Kwok, *Mol. Cryst. Liq. Cryst.*, 2009, **507**(1), 41–50.
- V. Jayalakshmi, G. Hegde, G. G. Nair and S. K. Prasad, *Phys. Chem. Chem. Phys.*, 2009, **11**(30), 6450–6454.
- G. Hegde, A. R. Yuvaraj, W. Sinn-Yam and M. M. Yusoff, in *Macromolecular Symposia*, 2015, vol. 353, pp. 240–245.



- 17 M. Alaasar, M. Prehm, K. May, A. Eremin and C. Tschierske, *Adv. Funct. Mater.*, 2014, **24**(12), 1703–1717.
- 18 M. Alaasar, M. Prehm, M. Brautzsch and C. Tschierske, *J. Mater. Chem. C*, 2014, **2**(28), 5487–5501.
- 19 M. M. Naoum, A. A. Fahmi, N. H. Ahmed and G. R. Saad, *Liq. Cryst.*, 2015, **42**(9), 1298–1308.
- 20 M. M. Naoum, A. A. Fahmi, A. H. Abaza and G. R. Saad, *Liq. Cryst.*, 2014, **41**(11), 1559–1568.
- 21 M. Podruczna, A. Hofmańska, I. Niezgoda, D. Pocięcha and Z. Galewski, *Liq. Cryst.*, 2014, **41**(1), 113–125.
- 22 Z. Li, H. Wang, M. Chu, P. Guan, Y. Zhao, Y. Zhao and J. Wang, *RSC Adv.*, 2017, **7**(71), 44688–44695.
- 23 R. Hayes, G. G. Warr and R. Atkin, *Chem. Rev.*, 2015, **115**, 6357–6426.
- 24 J. E. S. J. Reid, F. Agapito, C. E. S. Bernardes, F. Martins, A. J. Walker, S. Shimizu and M. E. Minas da Piedade, *Phys. Chem. Chem. Phys.*, 2017, **19**, 19928–19936.
- 25 O. Palumbo, F. Trequattrini, M. A. Navarra, J. B. Brubach, P. Roy and A. Paolone, *Phys. Chem. Chem. Phys.*, 2017, **19**, 8322–8329.
- 26 K. Dong, X. Liu, H. Dong, X. Zhang and S. Zhang, *Chem. Rev.*, 2017, **117**, 6636–6695.
- 27 D. Andrienko, *J. Mol. Liq.*, 2018, **267**, 520–541.
- 28 D. D. Díaz, D. Kühbeck and R. J. Koopmans, *Chem. Soc. Rev.*, 2011, **40**(1), 427–448.
- 29 M. Ikeda, R. Ochi and A. W. I. Hamachi, *Chem. Sci.*, 2010, **1**, 491–498.
- 30 M. A. C. Stuart, W. T. Huck, J. Genzer, M. Müller, C. Ober, M. Stamm and F. Winnik, *Nat. Mater.*, 2010, **9**(2), 101.
- 31 X. Chen, J. Gao, B. Song, M. Smet and X. Zhang, *Langmuir*, 2009, **26**, 104–108.
- 32 K. Stappert, J. Muthmann, E. T. Spielberg and A. V. Mudring, *Cryst. Growth Des.*, 2015, **15**(9), 4701–4712.
- 33 L. J. Yu, R. G. Peng, Y. Z. Wang and Y. K. Yang, *Adv. Mater. Res.*, 2012, **534**, 122–125.
- 34 H. Tamura, Y. Shinohara and T. Arai, *Chem. Lett.*, 2010, **39**, 240–241.
- 35 S. Zhang, S. Liu, Q. Zhang and Y. Deng, *Chem. Commun.*, 2011, **47**, 6641–6643.
- 36 J. Avó, L. Cunha-Silva, J. Lima and A. Jorge Parola, *Org. Lett.*, 2014, **16**, 2582–2585.
- 37 J. Yang, H. Wang, J. Wang, Y. Zhang and Z. Guo, *Chem. Commun.*, 2014, **50**, 14979–14982.
- 38 S. Shi, T. Yin, X. Tao and W. Shen, *RSC Adv.*, 2015, **5**, 75806–75809.
- 39 A. Wu, F. Lu, P. Sun, X. Gao, L. Shi and L. Zheng, *Langmuir*, 2016, **32**, 8163–8170.
- 40 E. Madihlagan, B. N. Sunil, Z. Ngaini and G. Hegde, *J. Mol. Liq.*, 2019, **292**, 111328.
- 41 N. Trbojevic, J. C. Haenle, T. Wöhrle, J. Kirres and S. Laschat, *Liq. Cryst.*, 2016, **43**(8), 1135–1147.
- 42 W. J. Goodby, *Handbook of Liquid Crystals Set*, 1998, pp. 411–440.
- 43 M. L. Rahman, G. Hegde, M. M. Yusoff, M. N. F. A. Malek, H. T. Srinivasa and S. Kumar, *New J. Chem.*, 2013, **37**(8), 2460–2467.

